University of Stavanger

Faculty of Science and Technology

MASTER'S THESIS

Study program/ Specialization: **MSc Petroleum Engineering / Drilling Technology**	Spring semester, 2015 **Open**
Writer: **Håvard Stangeland**	..... (Writer's signature)
Faculty supervisor: **Mesfin Belayneh and Bernt S. Aadnøy**	
Title of thesis: **Experimental Lost Circulation and Performance Simulation Studies of 60/40, 70/30, 80/20 and 90/10 OBMs**	
Credits (ECTS): **30**	
Key words: OBM Bridging Rheology Lost Circulation Hole cleaning	Pages: 98 Stavanger, 15.06.2015

Abstract

Lost circulation has been and still is a cost factor for the drilling industry. By using lost circulation material in drilling fluid, it is possible to mitigate unnecessary loss of drilling fluid.

This thesis presents characterization, performance simulation and lost circulation performances of four types of oil based mud systems. These are of 60/40, 70/30, 80/20 and 90/10 oil-water ratio. The characterization part deals with rheology measurement and modelling at various temperatures, and is based on direct experimental measurements. The performance simulation study deals with the hole cleaning efficiency of the drilling fluids. The lost circulation part deals with the bridging performance of the drilling fluids at various simulated fracture widths. For the experiment, 13.82 lb/bbl LC-lube (graphite) was used as lost circulation material.

The results show that particle size distribution with a D50 at or higher than the fracture width gives a better performance in terms of bridge strength. Similar results have also been documented in previous works. For the studied mud systems, three rheological parameters also show good correlation with the bridge collapse pressure.

Acknowledgements

I would like to thank associate professor Mesfin Belayneh for his guidance, support and encouragement during my master's thesis. He has been available for good theoretical discussion as well as providing knowledge about the operation of the technical equipment.

I would also like to thank professor Bernt S. Aadnøy for allowing me to use his laboratory during my experimental tests.

I owe a great amount of gratitude to my fellow master students, Therese Vu, Annbjørg Fiveland and Veronica Hauge for great company and support throughout the semester.

And a last thanks to MI-SWACO for providing me with the mud systems used in the thesis work.

Table of contents

List of figures

List of tables

List of symbols

d	–	Depth of formation
E	–	Young's modulus
g	–	Gravitational constant
dh	–	Vertical thickness of formation
k	–	Consistency index
n	–	Flow behavior index
N	–	Total number of peaks
$P_{p\text{-}avg}$	–	Average peak pressure
P_{max}	–	Maximum pressure
P_{wf}	–	Fracturing pressure
P_{avg}	–	Average pressure
ΔP	–	Excess pressure within the fracture
P_o	–	Pore pressure
R	–	Radius of fracture
w	–	Width of fracture
σ_H	–	Maximum horizontal stress
σ_h	–	Minimum horizontal stress
σ_v	–	Vertical/overburden stress
σ_x, σ_y	–	In-situ stresses along the x- and y directions
ρ_b	–	Bulk density of formation
γ_g	–	Specific gravity of formation
ν	–	Poissons's ratio
β	–	Biot's constant
τ	–	Shear stress
γ	–	Shear rate
μ	–	Newtonian viscosity
τ_y	–	Yield stress
μ_p	–	Plastic viscosity
γ^*	–	Geometric mean of the shear rate
τ^*	–	Geometric mean of the shear stress
τ_{yL}	–	Low-shear yield point
A, B, C	–	Robertson-Stiff Model parameters

Abbreviations

NPT	–	Non-productive time
LCM	–	Lost circulation material
ECD	–	Equivalent circulating density
FCS	–	Fracture closure stress
PSD	–	Particle size distribution
IPT	–	Ideal packing theory
OBM	–	Oil based mud
PV	–	Plastic viscosity
AV	–	Apparent viscosity
YS	–	Yield stress
RPM	–	Revolutions per minute
OWR	–	Oil-water ratio
SEM	–	Scanning electron microscope
BHA	–	Bottom hole assembly

1. Introduction

In order to drill an oil- or gas well successfully, a continuous circulation of drilling fluid is required. The drilling fluid provides several functions, such as transportation of rock cuttings to the surface, lubrication and cooling of both the drill string and the drill bit, exert hydrostatic pressure in the well (Economides et al., 1998; Bourgoyne et al., 1991). The drilling fluid used should cause no side effects that could harm the well construction process. Meaning it should not damage the productive formation, lead to risks related to the health and safety of the personnel or contaminate the environment (Economides et al. 1998).

A typical pressure plot for a well is shown in Figure 1. When drilling a well, the pressure caused by drilling fluid in the well has to be kept in balance with the formation pressure in order to minimize the borehole problems (Aadnøy, 2010). Well problems such as stuck pipe and borehole collapse can occur if the mud weight is too low. By having a high mud weight there is a risk that the hole pressure will become larger than the fracture pressure of the formation. If this were to happen, the formation would start to crack and drilling fluid could be lost to the formation. This is what is defined as lost circulation in the drilling industry (Aadnøy, 2010). A huge drilling fluid loss increases both the operational cost and the non-productive time. In addition, the loss will cause damage to the formation. Depending on the intensity of the fluid loss, it is common practice to use pill systems, which are formulated from various particle additives. The performance of the particle additives should be tested and investigated from laboratory works.

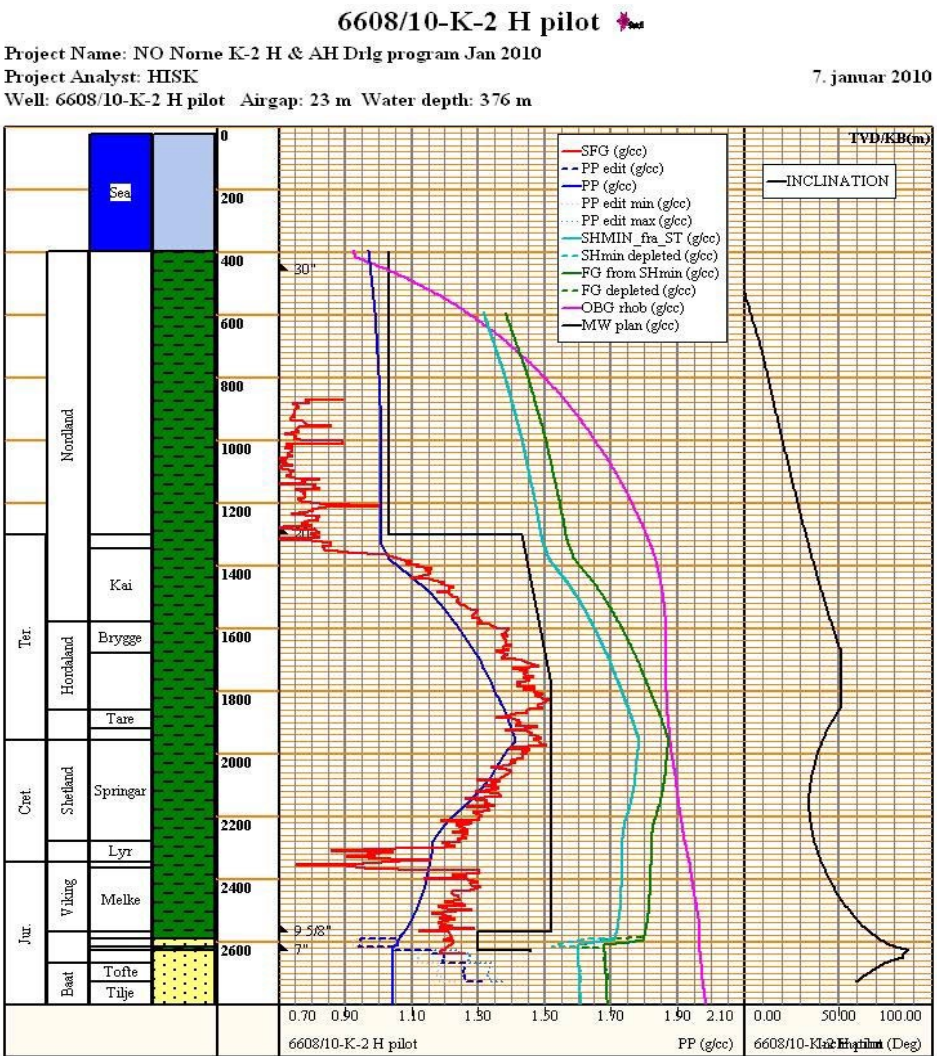

Figure 1: Pressure gradient plot for a well in the Norne field. (Statoil ASA, 2010).

1.2. Background of the thesis

As mentioned in the previous section, during drilling operations, there are several types of problems that can occur. Some of these are stuck pipe, lost circulation, borehole instability, pipe failures, formation damage (Azar and Robello Samuel, 2007). As mentioned above, each of these problems can lead to significant high non-productive time (NPT), which in return leads to a high additional cost of the operation. By designing an appropriate mud density and fluid properties it is possible to control the well instability problems to a certain degree.

Lost circulation can occur during different scenarios. The loss of fluid into the formation occurs when drilling into permeable or cavernous zones, and fractures that are natural or induced. In order to combat this problem, various remedial and preventative measures have been developed. One of these methods is the application of particle additives known as lost circulation material (LCM) in the drilling fluid, which increases the strength of the formation. The bridging agents also prevent the loss of circulation by plugging the pore- and fracture channels of the formation.

Numerous studies have been performed at the University of Stavanger on lost circulation since 1996. By the use of water-based mud systems, Toroqi (2012) performed experimental works for fracture sealing performance study at the University of Stavanger. Both Gerner (2012) and Khaing (2014) looked at the bridging performance of different oil-based muds when combined with a LCM. These two studies oil-water ratio of these muds were 60/40 and 80/20 for Gerner, and 70/30 and 90/10 for Khaing. Gerner used the same density for the mud systems, while Khaing had different density for the mud systems.

1.2. Problem formulation

In the previous studies, the effect of rheology on lost circulation performance was not studied in detail. Four oil-based mud systems will be used for the experimental and performance studies, and are shown in Figure 2. With a constant density of the four mud systems, it will be possible to look into the effect of the rheological properties of the fluid, and how it affects lost circulation.

Figure 2: Illustration of the 60/40, 70/30, 80/20 and 90/10 oil based mud systems.

The issues can be presented as:

- What is the bridging performance of oil based muds with different oil water ratio?
- How does temperature affect the rheology of the drilling fluids?
- Is there any correlation between the rheology of the fluids and the bridge collapse pressure?

1.3. Objectives

The objectives of this thesis are:

- Literature study of rheology models, lost circulation and fracture models.
- Rheology measurements of four oil based mud systems.
- Lost circulation experiments of the four mud systems.
- Analysis of the data from the rheology and lost circulation experiments.
- Performance evaluation of the mud system through simulation.
- Investigate if there is any correlation between the rheology parameters and pressure data from the lost circulation experiments.

2. Literature review

2.1. Lost circulation

One of the major drilling problems in the industry is lost circulation, which can occur in any operation where a fluid is pumped into the well. The loss of fluids occurs when two conditions are present; there has to be a formation with flow channels that allows fluid to flow from the well and into the formation, and the fluid present in the wellbore has to be in overbalance. Both of these conditions must be present for a lost circulation scenario to occur, but the type of lost circulation scenario will be dependent on which of these conditions are predominating (Mitchell and Miska, 2011). There are four main scenarios that are listed in Table 1 and illustrated in Figure 3.

Table 1: Four main scenarios for lost circulations (Mitchell and Miska, 2011).

Permeable zones	Rocks with high porosity and permeability will allow fluid to easily flow into the formation. Examples of such formations are unconsolidated formations and gravel beds.
Natural fractures	Naturally occurring secondary porosity and permeability, such as horizontal and vertical fractures in sandstone, shale and carbonate. These act as a flow path for the fluid in the wellbore.
Induced fractures	Fractures that are induced by having a well pressure that is higher than the fracture pressure of the rock. This kind of scenario is typically encountered during operations such as drilling and cementing.
Caverns	Formations with void space, which may be the result of limestones being leached by water.

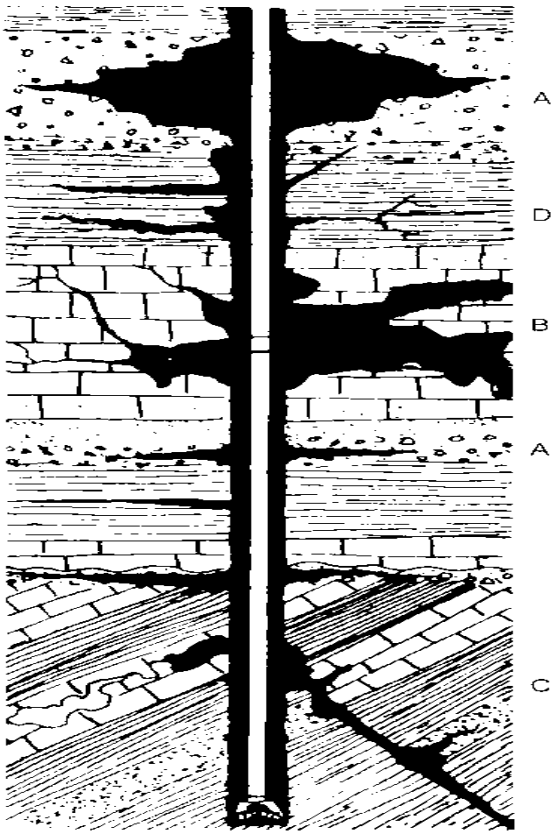

Figure 3: Lost circulation scenarios: A) Permeable zones, B) Caverns, C) Natural fractures, D) Induced fractures (Mitchell and Miska, 2011).

Lost circulation has a big economical impact on the drilling industry annually, as it affects the oil companies indirectly by causing an additional cost of hundreds of millions US dollars to the planned operations. In the time period 1990-1993, six wells in the North Sea were evaluated for a cost analysis, in order to look for improvements during the operations (Aadnøy, 2010). The borehole stability problems encountered during the pre-drilling of the wells are shown in Figure 4. It is seen that out of the total NPT, lost circulation is one of the greatest challenges.

Event	Time used (days)
Circulation losses	15
Tight hole	2
Squeeze cementing	15
Stuck casings	20
Fishing	2
Total	52 days
Per well	52/6 = 8.7 days

Figure 4: Time lost due to borehole instability problems for 6 wells in the North Sea.

Due to the high costs of lost circulation, the industry has focused on mitigating the conditions that causes the lost circulation situation to occur. The mitigation of lost circulation can be divided into preventative measures and remedial measures, which will be discussed further in the next sections.

2.1.1. Preventative measures

In order to prevent or reduce the effect of lost circulation, there are three areas in the drilling operation that should be focused on (Mitchell and Miska, 2011):

- Mud system design
- Equivalent circulating density (ECD) monitoring
- Selective casing design

The ECD has to be monitored in order to make sure that the well pressure is within the pore pressure and fracture pressure interval, although the mud weight may be correct, the ECD also takes the frictional pressure into account. Therefore the mud weight is not the only parameter affecting the well pressure, but also the rheological properties of the mud has to be maintained in order to circulate the well at an optimal pump rate.
The setting depth of the casing is planned in order to protect the weaker formations closer to the surface against the mud weight required at deeper well sections. It should also be ensured that the casing points are not located in potential loss zones.

The two discussed areas might not be enough to prevent a lost circulation scenario, which in turn makes the type of mud system important. There will be some cases where the well cannot be drilled effectively and safely with a conventional mud system, and it may therefore be a need of a different mud system, which allows underbalanced drilling for example. The selection of mud system will be dependent on local drilling conditions and well parameters that denotes the extent of overbalance required, formation pressure, and risk of abnormal or unexpected conditions.

2.1.2. Remedial measures

In cases where lost circulation has already occurred, there are measures for preventing the situation from developing further, by either controlling the lost circulation or by attempting to seal off the interval where there is loss of circulation (Mitchell and Miska, 2011). These measures includes:

- Removal of the conditions that causes the lost circulation, thereby allowing the formation to heal itself
- Bridging off the lost circulation interval by adding lost circulation material (LCM) or drilled solids
- Spotting a high-viscous plug across the interval
- Squeeze cementing in the interval
- Setting pipe across the interval
- Either abandon or sidetrack the interval

The type of measure, or in some cases the combination of the measures will be selected based on the location, type and severity of the problem.

2.2. Rock mechanics

In order to understand the fracture theories, it is important to have some knowledge about the terms used in solid mechanics theory, which are applied to the study of rock mechanics. The content of this part will be based upon the book "Petroleum Rock Mechanics" written by Looyeh and Aadnøy (2011). In this thesis, the main focus will be on the interaction of stress and strain on the subsurface rock formations. The terms that will be defined in detail are:

- In-situ stresses
  - Maximum horizontal stress (σ_H)
  - Minimum horizontal stress (σ_h)
  - Vertical/overburden stress (σ_v)

2.2.1. In-situ stresses

In-situ stress or far-field stresses are the natural occurring stresses that formations are exposed to subsurface. At any given point subsurface, there will be three perpendicular stresses that exist, which are the minimum horizontal stress, the maximum horizontal stress and the vertical stress. The effect of the vertical stress is mainly from the weight of overlaying deposit, but it can also come from geological events such as either magma or salt dome intrusion in the immediate area. The overburden stress interferes with the underlying rocks, causing them to spread and expand in a lateral direction, as a result of Poisson's effect. The horizontal stresses will then form due to the restriction of the lateral movement caused by the adjacent material.

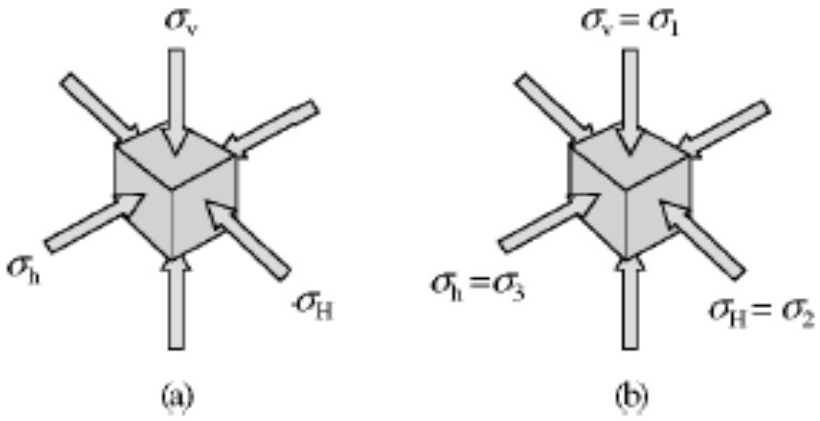

Figure 5: Illustration of in-situ stresses in a) Rock formation and b) drilled formation (Looyeh and Aadnøy, 2011).

2.2.2. Vertical stress

Since the vertical stress has now been defined, it can be expressed as:

$$\sigma_v = \int_0^d \rho_b(h) g dh \qquad (1)$$

Where, ρ_b = bulk density of formation

g = gravitational constant

d = depth of formation

dh = vertical thickness of formation

If the specific gravity of the formation is known, from density logs, it is possible to find the overburden stress in psi by using the following equation:

$$\sigma_v = 0.434 \gamma_g d \qquad (2)$$

Where

γ_g = specific gravity of formation

2.2.3. Horizontal stresses

While it is rather easy to establish the vertical stress, by using density logs, it is more complicated to determine the two horizontal stresses. As mentioned, the two horizontal stresses are dependent on the vertical stress, but they can also be the result of other geological events. Thus, an empirical equation was proposed by Avasthi et al. (2000), where geological events are neglected, and only vertical stress is accounted for. The equation is defined below, and by accounting for only vertical stress, the horizontal stresses will have the same magnitude, since they are both perpendicular to the overburden stress, as shown in Figure 5.

$$\sigma_h = \sigma_H = \frac{v}{1-v}(\sigma_v - \beta P_o) + \beta P_o \quad (3)$$

Where
v = Poisson's ratio
β = Biot's constant
P_o = pore pressure

2.3. Fracture models

Since lost circulation is a problem related to the well fracture model, this section will review the different models in detail. Well fracture occurs when the pressure in the well exceeds the fracture strength of a wellbore. When the fracture has developed, loss of mud to the formation will follow. The well fracture models are derived based on the boundary conditions at the wellbore and the mode of deformation.

The linear elastic fracture model uses the Kirsch equations in order to determine the fracture initiation pressure. According to the model, fracture will occur in the well when there is a change in the rock stress, from compression to tension. This change in the stress occurs when the borehole pressure exceeds the minimum horizontal stress. At a larger wellbore pressure, the hoop stress will be significantly reduced, making it fall below the tensile strength of the rock.

The model can be analysed by assuming boundary conditions at the wellbore. These are non-penetrating fluids and penetrating fluids.

2.3.1. Non-penetrating well fracture model

The non-penetrating model is based around the assumption that the boundary condition at the wellbore is non-communicating. The model assumes a steep transition between the well pressure and pore pressure, as illustrated in Figure 6.

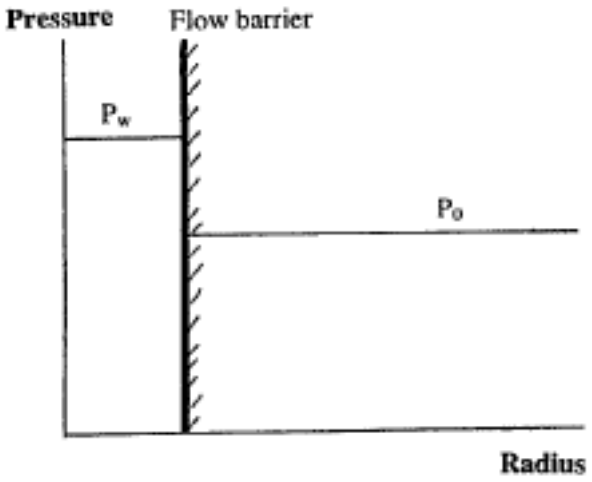

Figure 6: Pressure distribution for non-penetrating case (Aadnøy, 1998).

The non-penetrating fluids contain filtrate control that will form a filter cake in order to prevent fluid from escaping the wellbore. The fracture pressure for non-penetrating fluids can be defined as:

$$P_{wf} = 3\sigma_y - \sigma_x - P_o \qquad (4)$$

Where

P_{wf} = fracture pressure

σ_x, σ_y = in-situ stresses along the x-and y directions

2.3.2 Penetrating well fracture model

The penetrating model assumes that the boundary condition at the wellbore is penetrating. Hence, there is a communication between the wellbore and the formation.

As illustrated in Figure 7, the drilling fluid is free of filtrate control, and does not make a suitable filter cake. The fluid is then able to penetrate the wellbore wall and invade the rock formation. From the figure, it can be seen that the pore pressure is building up at the wellbore wall. Well pressure and pore pressure are equal at the wellbore.

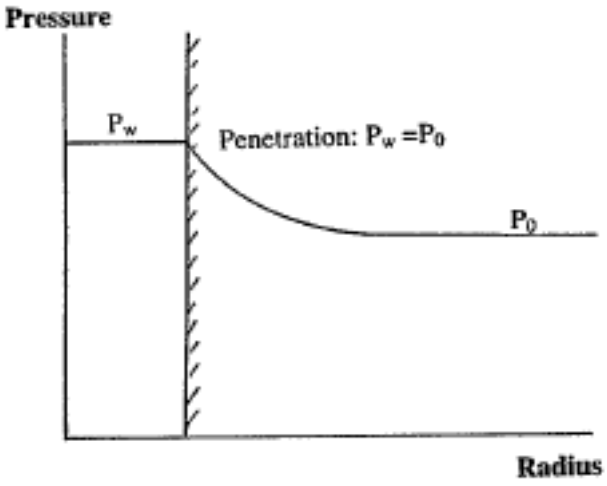

Figure 7: Pressure distribution for penetrating case (Aadnøy, 1998).

By assuming isotropic in-situ stress condition, equation (4) is reduced to:

$$P_{wf} = \sigma_h \tag{5}$$

2.4. Stress Cage

Stress cage is considered as a method of strengthening the wellbore by increasing the fracture resistance of the formation. The concept behind stress cages is that small fractures are induced, and thereafter introduced to particles in the mud that allows the fracture to stay open, but sealed. If the fracture is properly sealed near the wellbore, there will be an increase in the hoop stress around the wellbore (Aston et al., 2004).

2.4.1. Bridging

To achieve the wanted strengthening effect, the particles added to the drilling fluid have to be proper size in order to enter the fracture. After the particles have entered the fracture, a bridge will start to form. The bridge will act as both a proppant and a seal, which isolates the pressure inside the wellbore from the fracture. If the permeability of the formation is higher than that of the bridge, the fluid behind the bridge will start to dissipate (Alberty and McLean, 2004). This progression is shown in Figure 8. The tip of the fracture will then start to close, as the pressure behind the bridge reaches equilibrium.

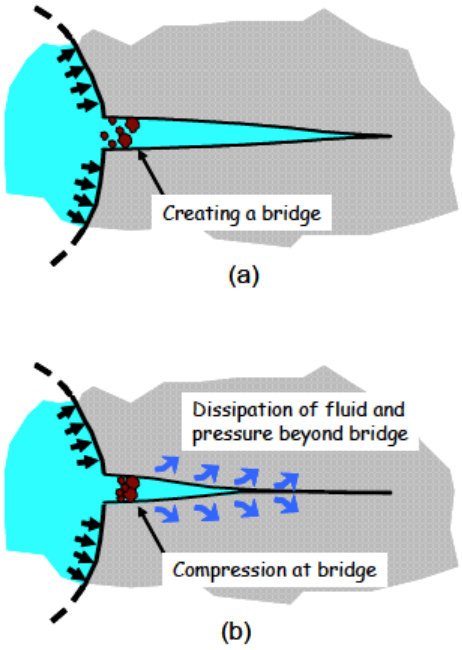

Figure 8: Process of bridging. (a) Particles gather at the mouth of the fracture, creating a bridge. (b) Fracture closes as the pressure reaches equilibrium (Alberty and McLean, 2004).

2.4.2. The strengthening process

As mentioned earlier, a fracture will initiate when the rock stress goes from compression into tension. The stress that tries to close the fracture is an important term to understand, which is called the fracture closure stress (FCS). For a fracture that is fully closed, there will be a certain pressure required to open the fracture. This pressure will be equal to the FCS. Furthermore, in order to reopen an already induced fracture, the fracture re-opening pressure will have to be obtained. This means that the fracture will start to gain width when the FCS is reached, which is equal to the fracture re-opening pressure. The FCS will have an increase in value due to the particles that are trapped in the fracture. This increase is caused by the compression of the surrounding formation when the fracture is widened (Dupriest, 2005).

The principle behind increasing the FCS is that fluid losses will stop if the circulating pressure is less than this stress. The fracture will then be sealed and kept open, by the help of the particle bridge. Therefore, it will be safe to drill with a circulating pressure as long as it is below the newly obtained FCS.

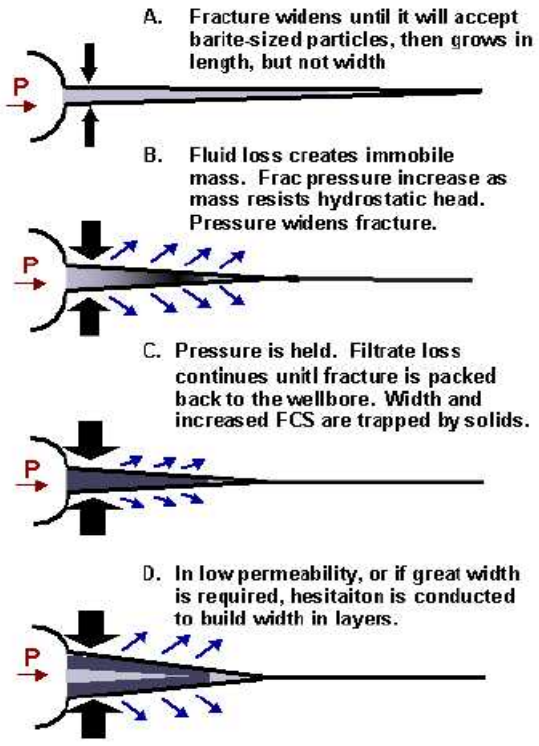

Figure 9: Strengthening process of wellbore (Dupriest, 2005).

2.5. Particle size distribution

The particle size distribution (PSD) is used to denote the amount of different sized particles that are contained in a mud, with the purpose of minimizing the mud loss.

2.5.1. Abrams' 1/3 rule

Through laboratory tests, Abrams discovered that an effective bridging would occur if the median particle size was greater than 1/3 of the median pore size. In addition, the amount of bridging particles in the mud should be more than 5% of the total volume of solids (Abrams, 1977).

2.5.2. Vickers method

The Vickers method is based upon five criteria for the bridging particles in the mud in order to establish a good PSD that will reduce the amount of fluid loss. Five parameters must be known in order to perform the Vickers method, which are the D90, D75, D50, D25 and D10 of the pore throat distribution. The criteria are stated below (Vickers et al., 2006):

- D90 = Largest pore throat
- D75 < 2/3 pore throat
- D50 +/- 1/3 of the mean pore throat
- D25 1/7 of the mean pore throat
- D10 > smallest pore throat

2.5.3. Ideal packing theory

The PSD achieved by using the ideal packing theory (IPT) gives a particle range that will seal both the pores and the void space created by the bridging particles. For this method, the pore size or fracture width should be known. However, if there is a lack of this data, it is possible to use the permeability of the formation in order to estimate the distribution of pore size.

In order to determine if the packing of the particles are ideal, the percent of cumulative volume is plotted against the square root of the particle diameter ($D^{1/2}$). Ideal packing is achieved if a straight line is formed (Dick et al., 2000).

2.5.4. Halliburton method

This method was developed when Don Whitfill did studies on PSD and fracture width. When the fracture width is known, or estimated, the PSD can be optimized in order to create a bridge. The PSD will then be set with a D50 equal to the fracture width, in order to ensure that both smaller and larger particles will provide a seal of the fracture. In order to estimate fracture width, the following equation was presented in the paper (Whitfill, 2008):

$$\Delta P = \frac{\pi}{8} * \frac{w}{R} * \frac{E}{(1-\nu^2)} \quad (6)$$

Where

ΔP = Excess pressure within the fracture

w = width of fracture

R = radius of fracture

E = Young's modulus

ν = Poisson's ratio

2.6. Drilling fluid

2.6.1. Types of drilling fluid

Currently in the industry, there are four common types of drilling fluids available, which are (Economides et al., 1998):

- Water-based mud
- **Oil-based mud (OBM)**
- Synthetic-based mud
- Pneumatic drilling fluids

These fluids are affected by temperature and pressure variations, which in turn has an effect on the physical and visco-elastic properties and the rheology. The performance of the drilling fluid is therefore influenced by these changes.

Oil-based mud

Since oil-based mud is the mud system used in this thesis, the other types of fluids will not be discussed in further detail. Oil-based mud is known for having good inhibitive properties against shale formations and granting drill string lubrication, which both assists in providing a good drilling performance. The chances of experiencing drilling related problems such as corrosion and stuck pipe can be reduced and to some degree avoided by using oil-based mud (Skjeggestad, 1989).

This kind of mud is very effective when drilling in scenarios such as; highly reactive shale and evaporite, as long as the salinity of the emulsified water is higher than the salinity of the water in the formation (Skjeggestad, 1989), extended reach wells, and high-pressure, high temperature wells exposed to hydrogen sulfide (H_2S), which will get neutralized due to the high content of calcium hydroxide ($Ca(OH)_2$) in OBM. (Skjeggestad, 1989; Economides et al., 1998).

2.6.2. Drilling fluid additives

In zones where a loss of fluid to formation is expected, there may be a need to add additional material in order to address the lost circulation. In some cases it will be enough to let the cutting transport create a bridge to seal off the interval, but it is often necessary to provide lost circulation material (LCM) to the mud. The LCM is a type of material that is designed specifically to prevent major fluid loss, and should typically not exceed a concentration of 10 to 20 lbm/bbl (ppb). Examples of lost circulation material are listed below (Mitchell and Miska, 2011):

- Fibrous materials
    - Wood fiber
    - Cotton fiber
    - Animal hair
    - Shredded tires
- Granular materials
    - Nut shells
    - Seed grains
    - Bentonite
- Flaky materials
    - Mica
    - Cellophane
    - Plastic laminate
- **LC-lube**

LC-lube

LC-lube is a type of LCM that is designed to prevent and control loss of circulation, partial loss and seepage loss of different kinds of drilling fluids. It is composed of resilient graphite, with angular shape and different sized particles. The LC-lube is also inert, meaning that it does not interfere much with the rheology of the drilling fluid (at low concentrations) and the downhole logging tools. The LC-lube can be applied to both water- and oil-based drilling fluids, and in addition to act as a LCM it also reduces the torque and drag by acting as a lubricant (Baker Hughes, 2007).

Studies done by Savari et al. (2012) showed that the resilience of graphite is close to 120 percent at 10 000 psi. The other LCM that was tested during the studies showed zero or minimal resiliency for the tests at 5000 and 10 000 psi. What is unique about the graphite is that the resilient nature of the material allows it to be compressed and mold itself to the fracture tip when experiencing pressure. Afterwards when the pressure is released, the material will rebound, continuing to seal the fracture (Savari et al, 2012).

2.6.3. Properties of drilling fluids

Density

The density of a fluid is temperature and pressure dependant. This means that as the pressure is increased the density of the fluid will also increase, and as the temperature is increase there will be a decrease in the density of the fluid.

Viscosity

Viscosity can be described as the internal resistance to flow. The resistance to flow is caused by both mechanical friction and electrochemical forces between the molecules. The viscosity is dependant on several factors, such as temperature, pressure and the physical/chemical composition of the fluid.

Plastic viscosity

The plastic viscosity (PV) is the part of the flow resistance that is determined the mechanical friction in the fluid. The mechanical friction can be caused by the friction between the particles in the fluid as well as the friction between the liquid surface and the particles (Thorbjørnsen, 2009).

Apparent Viscosity

The apparent viscosity (AV) is the relationship between shear stress and shear rate, and provides information about the total viscosity of the fluid.

Yield stress

The yield stress (YS) is the part of the resistance that is developed due to the electrochemical forces between the molecules in the fluid (Thorbjørnsen, 2009).

YS/PV ratio

The ratio of yield stress to plastic viscosity is used as a measure of thinning of the fluid (Darley and Gray, 1988). When comparing fluids, a higher ratio will express a greater shear thinning.

2.7. Drilling fluid rheology and models

The term rheology is an expression used for the study of deformation and suspension properties of a flow in pipes or other conduits. In order to move the drilling fluid through the longer, slender pipes and annuli in the drilling process, the large viscous forces must be overcome.

A means to describe the flow behaviour can be done by the rheological model, which gives a description of the relationship between the shear rate and the shear stress. The Newtonian and non-Newtonian fluids are illustrated in Figure 10 below. Pseudoplastic (Power Law) is a shear thinning fluid, while dilatant is a shear thickening fluid:

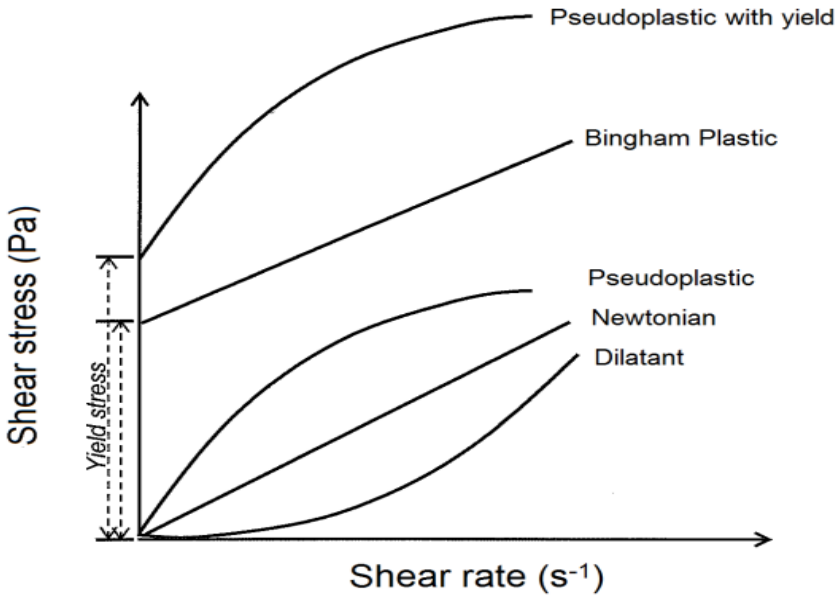

Figure 10. Rheological models for Newtonian and non-Newtonian fluids (Vieira et al., 2012).

2.7.1. Newtonian model

Newtonian fluids are fluids that do not contain particles greater than molecules, such as clean water, glycerin and oils. These fluids will exhibit a constant viscosity at any shear rate when the fluid is exposed to a constant pressure and temperature.

Therefore, by plotting shear stress versus shear rate for a Newtonian fluid, a straight line through the origin will be obtained. The model for Newtonian fluid can be described by the following equation (Skjeggestad, 1989):

$$\tau = \mu * \gamma \quad (7)$$

Where
τ = Shear stress
γ = Shear rate
μ = Newtonian viscosity

2.7.2. Non-Newtonian models

Non-Newtonian fluids contains particles with a size greater than molecules, an example is drilling fluids. The models used for Non-Newtonian fluids will be described in the following section.

2.7.2.1. Bingham plastic model

The Bingham plastic model is similar to the Newtonian model in a sense that the relationship between the shear stress and shear rate is linear. However, in order to initiate flow of the fluid, a finite stress is required. The finite stress is the yield stress. The model can be described by equation (8) (Skjeggestad, 1989; Caenn et al., 2011):

$$\tau = \tau_y + \mu_p * \gamma \quad (8)$$

Where
τ_y = Yield stress [lbs/100 ft^2]
μ_p = Plastic viscosity [cP]

These two parameters above can be calculated by equation (9) and (10) (Skjeggestad, 1989):

$$\mu_p = R_{600} - R_{300} \quad (9)$$

$$\tau_y = F_{300} - \mu_p \quad (10)$$

2.7.2.2. Power law Model

The Power law model can be used in order to describe pseudoplastic fluids, which are fluids that have a reduction in viscosity as the shear rate increases. This model is better at describing fluids than the Bingham plastic model, especially at lower shear rates. The equation used to describe the model is (Skjeggestad, 1989; Mitchell and Miska, 2011):

$$\tau = k\gamma^n \quad (11)$$

Where
k = Consistency index
n = Flow behavior index

The value of n will determine what flow model the power law describes (Caenn et al., 2011):

- n < 1, pseudoplastic fluid, effective viscosity decreases with shear rate.
- n = 1, Newtonian fluid, constant fluid viscosity
- n > 1, dilatant fluid, effective viscosity increases with shear rate

In order to find the n and k values, equation (11) is rewritten by taking the logarithm of each term, resulting in the following equation.

$$\log \tau = \log k + n \log \gamma \quad (12)$$

The equation is now linearized, and the n and k value can be found graphically, as the slope of the curve and intercept on the y-axis respectively.

The two values can also be estimated from Fann35 data, by using the following equations (Skjeggestad, 1989):

$$n = 3.32 \log\left(\frac{R_{600}}{R_{300}}\right) \tag{13}$$

$$k = \frac{R_{300}}{511^n} = \frac{R_{600}}{1022^n} \tag{14}$$

2.7.2.3. Herschel-Bulkley model

The Herschel-Bulkley model applies the characteristics of both the Bingham and Power-law model, and uses three parameters in order to characterize a fluid. The model is defined by equation (15) (Mitchell and Miska, 2011):

$$\tau = \tau_y + k\gamma^n \tag{15}$$

It can also be rewritten by taking the logarithm of each term:

$$\log(\tau - \tau_y) = \log k + n \log \gamma \tag{16}$$

In order to obtain a value for τ_y, Versan and Tolga (2005) proposed the following approach, where $\tau_y = \tau_0$:

$$\tau_0 = \frac{\tau^{*2} - \tau_{min} * \tau_{max}}{2 * \tau^* - \tau_{min} - \tau_{max}} \tag{17}$$

Where

τ^* = Shear stress value that corresponds to the geometric mean of the shear rate, γ^*.

$$\gamma^* = \sqrt{\gamma_{min} * \gamma_{max}} \tag{18}$$

The τ^* is then found by interpolating the γ^* value with the shear stress values.

2.7.2.4. Unified model

The unified model is a new rheological model designed for the drilling industry, which is based upon the Herschel-Bulkley model (Zamora and Power, 2002). The equation is expressed below, with its linearized counterpart:

$$\tau = \tau_y + k\gamma^n \quad (19)$$

$$\log(\tau - \tau_y) = \log k + n \log \gamma \quad (20)$$

What differentiates the unified model from the Herschel-Bulkley model is how to estimate the yield stress, τ_y. Zamora and Power proposed the following method for solving yield stress, by taking τ_y as the low-shear yield point (τ_{yL}):

$$\tau_{yL} = (2R_3 - R_6)1.066 \quad (21)$$

Where
τ_{yL}= Low-shear yield point
1.066 = Conversion factor from laboratory units to field units

2.7.2.5. Robertson-Stiff model

The Robertson-Stiff model was proposed by Robertson and Stiff (1976) in an attempt to give a better description of the yield-pseudoplastic fluids. The model is defined as:

$$\tau = A(\dot{\gamma} + C)^B \quad (22)$$

Where
A, B and C = Model parameters

From equation (22), the parameters A and B act similar to the K and n parameters for the Power Law model. The C parameter is a correction of shear rate, where $(\dot{\gamma} + C)$ is considered as the effective shear rate.

By transforming equation (22) into the logarithmic form, it will be possible to achieve a straight line in a log-log plot.

$$\log \tau = \log A + B \log(\dot{\gamma} + C) \quad (23)$$

From equation (23) above, A will be the intercept and B will be the slope.

The last model parameter, C, can be found from the following equation:

$$C = \frac{\gamma_{min} * \gamma_{max} - \gamma^{*2}}{2\gamma^{*} - \gamma_{min} - \gamma_{max}} \quad (24)$$

Where

γ^{*} = Shear rate value that corresponds to the geometric mean of the shear stress, τ^{*}.

In order to find γ^{*}, the geometric mean of the shear stress must first be calculated, and then this value has to be interpolated with the values of shear rates. The equation used to find τ^{*} is shown below (Robertson and Stiff, 1976):

$$\tau^{*} = \sqrt{\tau_{min} * \tau_{max}} \quad (25)$$

2.8. Previous studies done on effect of rheology of fluid on lost circulation

In his PhD thesis, Toroqi (2012) tried to find a correlation between the sealing capability of a drilling fluid and its rheological properties. The maximum pressure from the lost circulation experiments were checked with various parameters such as PV, YS, AP. The results from his study indicated poor correlation, and it was concluded that the rheological parameters could not alone be used as an estimate of the sealing properties of a fluid.

3. Experimental setup and Materials

This chapter will cover the description of the experimental procedures, as well as apparatus and materials used. During this thesis, two laboratory experiments were performed:

- Rheology measurements to characterize the drilling fluids.
- Lost circulation experiment to study the performance of the different drilling fluids under same conditions.

Before these tests were conducted, the mud systems were sheared in the Hamilton Beach Mixer for about 15 minutes in order to ensure a proper homogeneous mixture.

3.1. Experimental apparatus

3.1.1. Fann35 Viscometer

The Fann35 viscometer measures shear stress at a certain shear rate. Shear stress is measured in the rates of 3, 6, 100, 200, 300 and 600 revolutions per minute (RPM). The shear rate (RPM) is converted into field units of s^{-1} by multiplying the values with 1.7023. The shear stress on the other hand is measured as deflection angle in °degrees, and is converted into field units of $lb/100ft^2$ by multiplying the values with 1.067.

The four drilling fluids were measured with the Fann35 viscometer at three different temperatures. The temperature phases that were used are 72°F, 120°F and 180°F. In order to achieve the higher temperature phases, a Tufel heating cup was used, and the temperature was monitored with a thermometer. The pressure condition for these experiments were all conducted at atmospheric pressure. The data obtained from the Fann35 viscometer will be presented later in the thesis.

3.1.2. Static bridge apparatus

The bridge apparatus used in this experiment is shown in a schematic overview in Figure 11. The system consists of a steel cylinder that is filled with mud. In order to simulate a fracture, steel slots are inserted at the bottom of the cylinder. Before the mud is placed inside of the steel cylinder, it is mixed with LCM in order to create a bridge at the fracture mouth as the particles settle.

The lower valve is closed, and the prepared mud is then filled inside of the cylinder. The top part of the cylinder is then attached, but the cylinder is still connected to atmospheric pressure through the opening on top. The high-pressure Gilson pump is then started, with a rate of 6 ml/min. The water pumped on top of the mud, in order to remove excess air in the cylinder. The cylinder is closed at the top part once water is observed at the opening. The pressure inside of the system can then be increased by the use of the pump.

The lower valve is then opened, and the experiment is conducted at a rate of 2 ml/min for 20 minutes. The pressure will build up as the particles added to the mud starts forming a bridge over the slot opening, and furthermore decrease once the bridge collapses. A computer is used in order to record the pressure measured by the pump, and is stored in Lab-View. The maximum pressure allowed for the system is 50MPa.

Four experiments will be conducted for each mud system, with varying slot sizes of 250µm, 300µm, 400µm and 500µm.

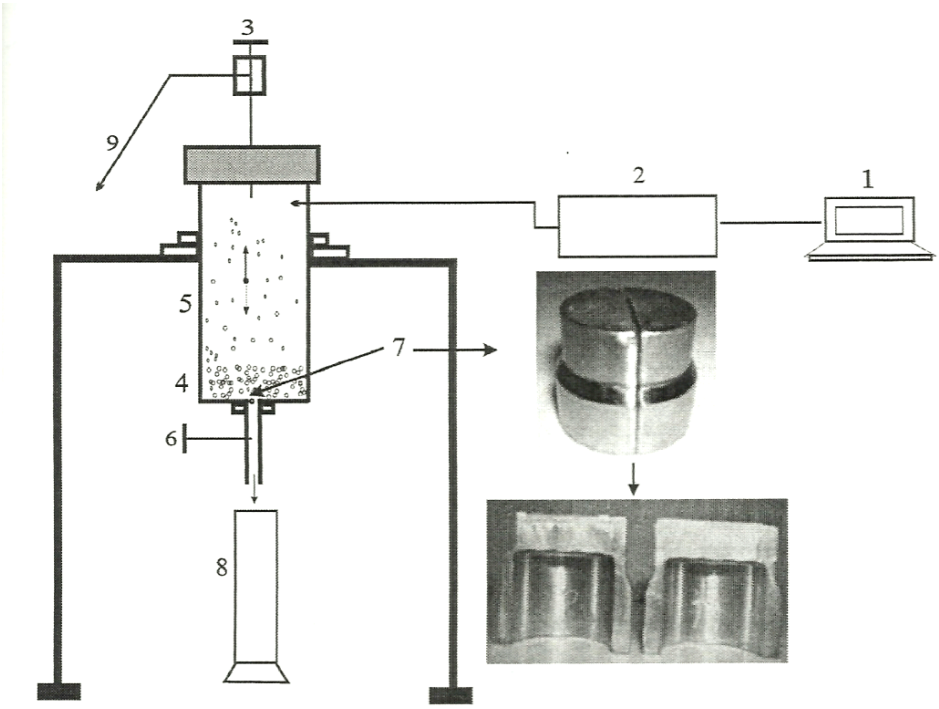

Figure 11: Schematic overview of the bridge apparatus (Belayneh, 2004).

3.2. Materials

3.2.1. Drilling fluids

For this thesis, four separate oil-based muds were used. The drilling fluids have different oil to water ratio, which are 60/40, 70/30, 80/20 and 90/10. These drilling fluids were provided by MI-SWACO.

In order to look into if the rheology has an affect on lost circulation, the drilling fluids have the same density of 1.75 specific gravity (s.g). The parameters of the mud systems will be explained in further details in later sections of the thesis.

3.2.2. Lost circulation material

For the lost circulation experiment, LC-lube was used, which consists of particles of varying sizes. The LC-lube particle solution was provided by Baker Hughes, and consists of resilient graphite. The particles have been sieved and distributed on beforehand, in order to create the mixture with a particles size distribution as shown in Figure 12.

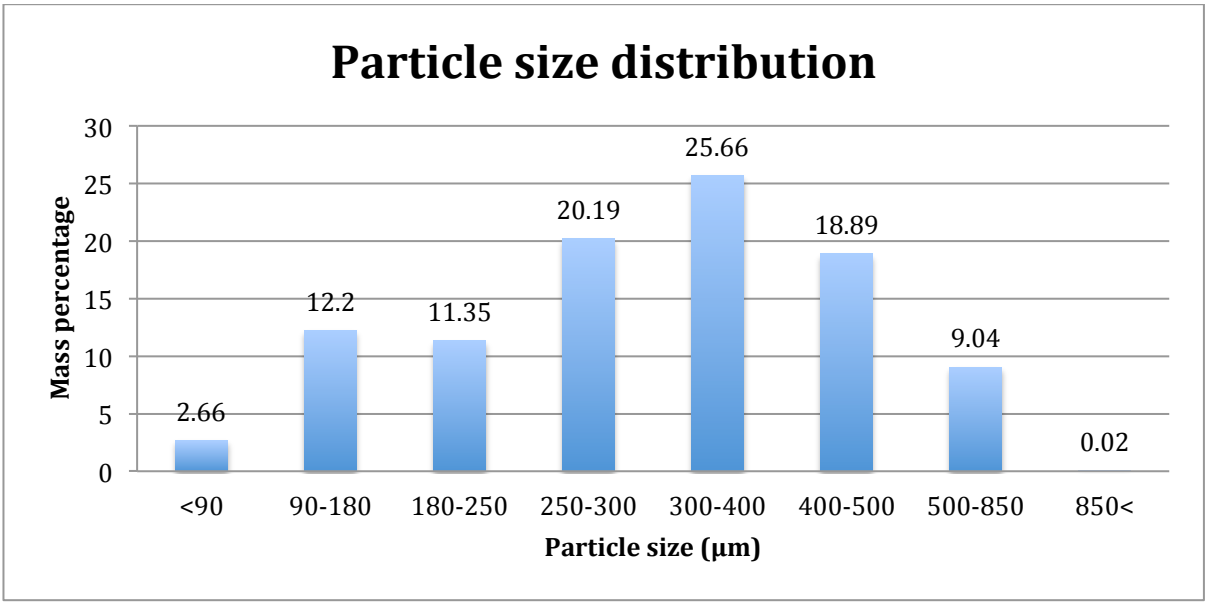

Figure 12: Particle size distribution of the LC-lube.

In order to assess the D10, D50 and D90 of the LC-lube, a curve with the cumulative percentage of the mixture has been plotted in Figure 13. The D10, D50 and D90 are estimated to be 150, 310 and 500 micron respectively. As one of the slot sizes used in the experiment is 300 microns, it corresponds with the Halliburton Method (Whitfill, 2008) that was mentioned Section 2.5.4. The effect of changing fracture width can therefore be investigated by using slot sizes that are both smaller and larger than the D50 of the PSD.

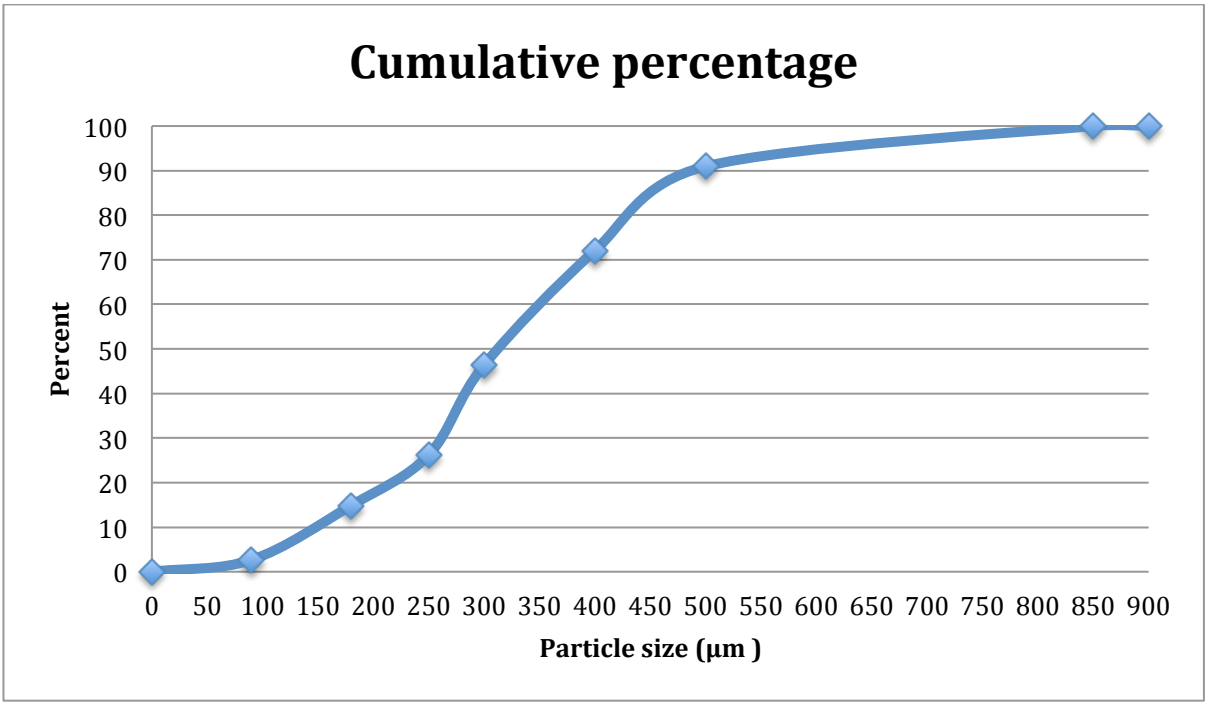

Figure 13: Cumulative percentage of the LC-lube mixture.

The structure of the particles can be seen in the scanning electron microscope (SEM) picture in Figure 14. It can be observed that the LC-lube consists of irregular shaped particles that are long in length with a smaller width.

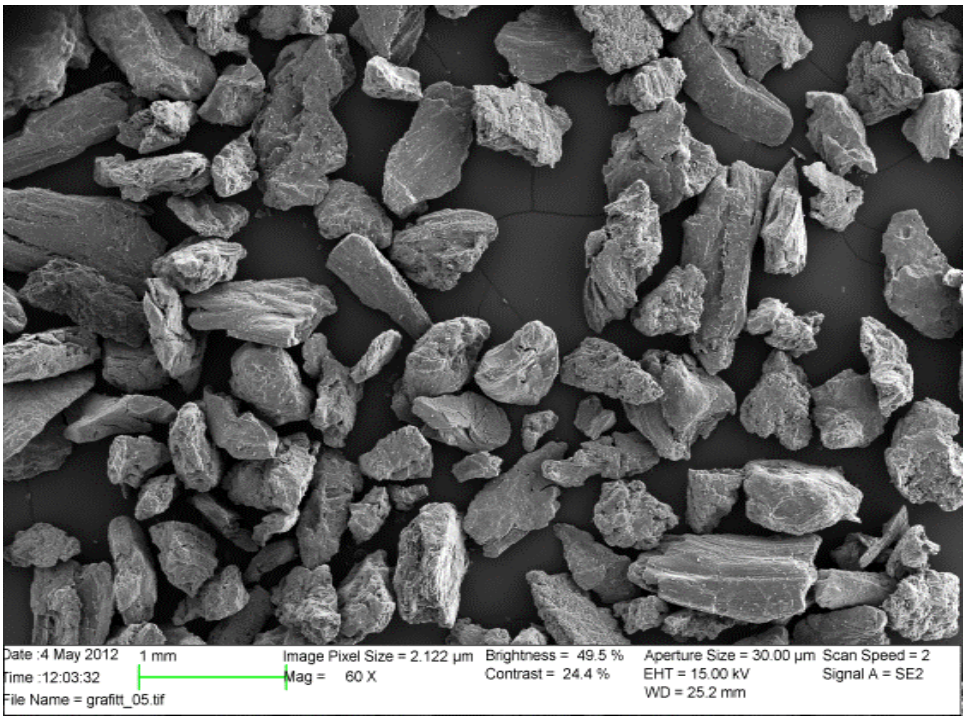

Figure 14: SEM picture of the LC-lube particles at a magnification 60X.

4. Results

4.1. Rheology measurements

The measurements from the Fann35 experiments at room temperature can be seen in Figure 15, as well as presented with the calculated rheological properties in Table 2.

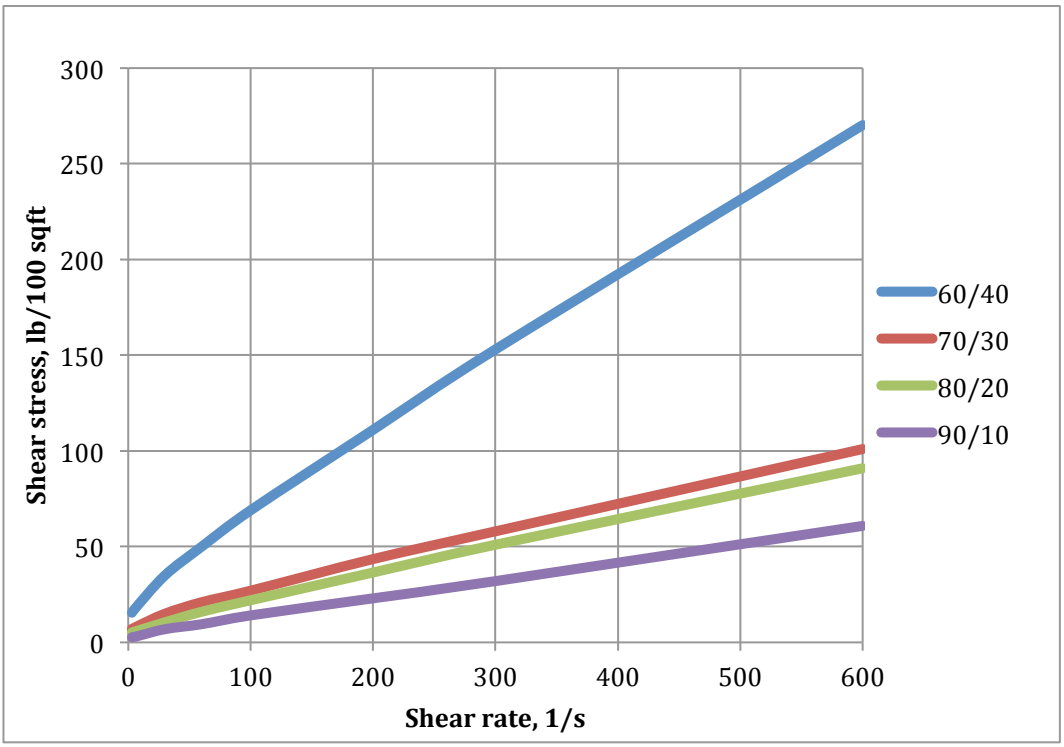

Figure 15: Drilling mud readings for 60/40, 70/30, 80/20 and 90/10 OBM.

There is a distinct difference in the measurements when looking at the 60/40 OBM and the three remaining OBMs, which can also be observed from the rheological properties.

Table 2: Fann35 data and rheology parameters for the OBMs.

Parameter	60/40 OBM	70/30 OBM	80/20 OBM	90/10 OBM
θ_{600}	270	101	91	61
θ_{300}	153	58	51	32
θ_{200}	111	43.5	36.5	23
θ_{100}	69	27	22	14.1
θ_{60}	50	21	16	9.5
θ_{30}	35	15	10.5	6.9
θ_{6}	18	8	5.8	3
θ_{3}	15.5	7	5.2	2.7
Apparent viscosity (cP)	135.0	50.5	45.5	30.5
Plastic viscosity (cP)	117.0	43.0	40.0	29.0
Yield stress (lb/100 ft^2)	36.0	15.0	11.0	3.0
YS/PV	0.31	0.35	0.28	0.10
Density (s.g)	1.75	1.75	1.75	1.75

4.2. Modelling and analysis of rheology

The parameters obtained from the rheology data are important for drill string mechanics, hydraulics ECD, hole cleaning, kick simulation and swab/surge calculations. As discussed earlier, there have been proposed several rheology models with the purpose of describing fluid behaviour. These models are not "tailor-fitted" for a certain kind of fluid, hence the mud systems used in this thesis will have to be analysed in order to decide which model is the best match.

The following subsections will delve into the measurements done for the Fann35 tests by applying them to the different rheological models, as well as a comparison of the errors obtained when the separate models are compared with the measurements.

Furthermore, the plastic viscosity and yield stress of the mud systems at different temperatures will be modelled and analysed. The data for each of the derived models can be found in appendix A, whereas some of it will be presented in the text.

4.2.1. Rheology Modelling and Analysis of 60/40 OBM

The different rheology models of the OBM with an oil-water ratio (OWR) of 60/40 at room temperature of 72°F is shown in Figure 16. The shear stress from the experimental data is recalculated into values for the separate models, and then compared.

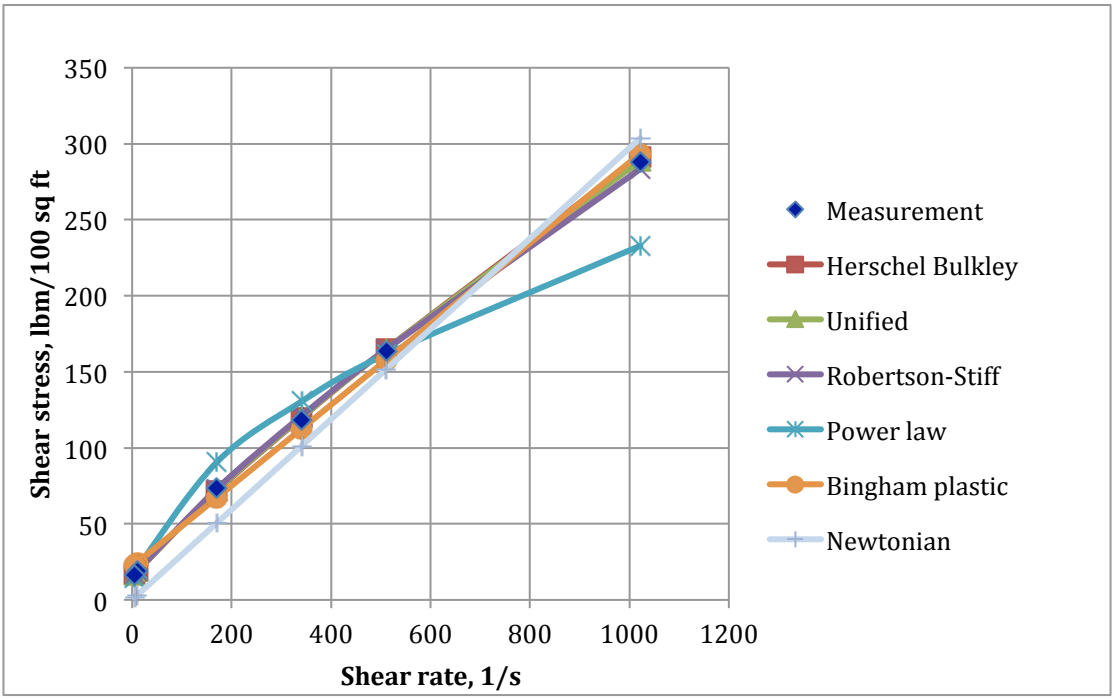

Figure 16: The different rheology models compared to measured data for the 60/40 OBM at room temperature.

In order to establish an error presented by the models, each model was compared to the original measurements. The error, shown in percentage for each model, can be found in Figure 17.

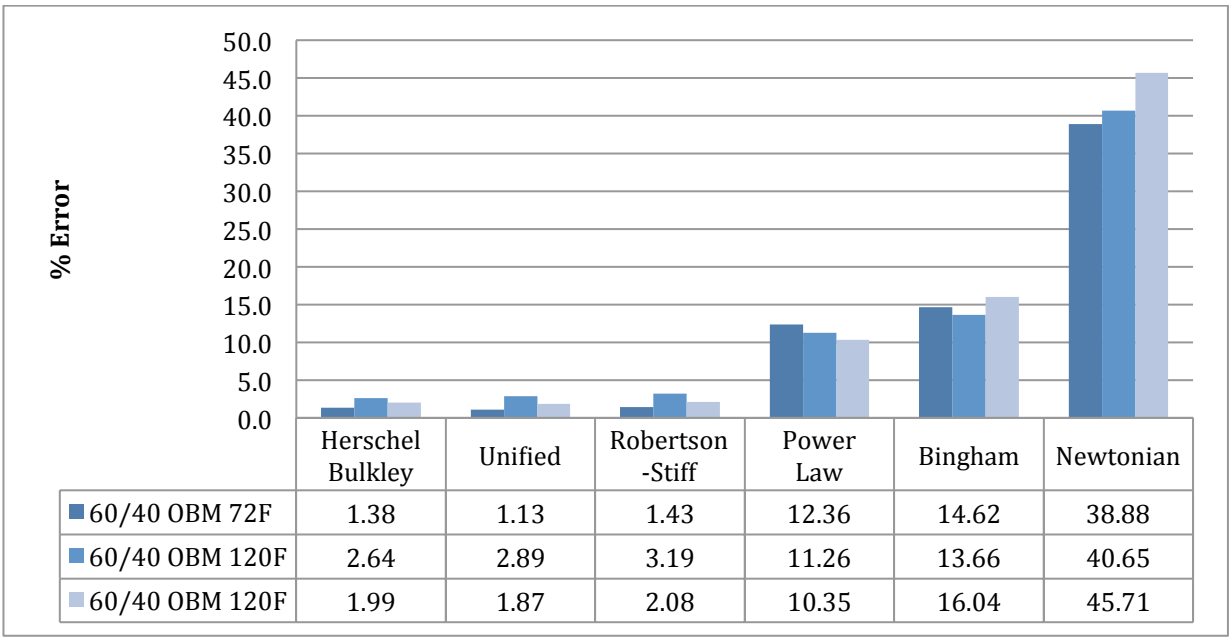

	Herschel Bulkley	Unified	Robertson -Stiff	Power Law	Bingham	Newtonian
60/40 OBM 72F	1.38	1.13	1.43	12.36	14.62	38.88
60/40 OBM 120F	2.64	2.89	3.19	11.26	13.66	40.65
60/40 OBM 120F	1.99	1.87	2.08	10.35	16.04	45.71

Figure 17: The error of the rheology models compared for the 60/40 OBM at 72, 120 and 180°F.

When comparing the error for the models with each other, it is observed that the Herchel Bulkley-, Unified- and Robertson-Stiff-model exhibit the lowest errors, all within the same threshold. These three models prove to give the best representation of the behaviour of the 60/40 mud system.

The Power law and Bingham models are also within their own threshold, but higher than the three models previously mentioned, giving a worse representation of the mud. The Newtonian model is significantly higher than the rest of the models, and is a poor model for describing the mud system.

It should also be noted that even though the temperature is increased, the error stays within the same range for the different models. Therefore, the accuracy of the models does not appear to be affected by a change in temperature.

4.2.2. Rheology Modelling and Analysis of 70/30 OBM

The different rheology models of the OBM with an oil-water ratio (OWR) of 70/30 at room temperature of 72°F is shown in Figure 18.

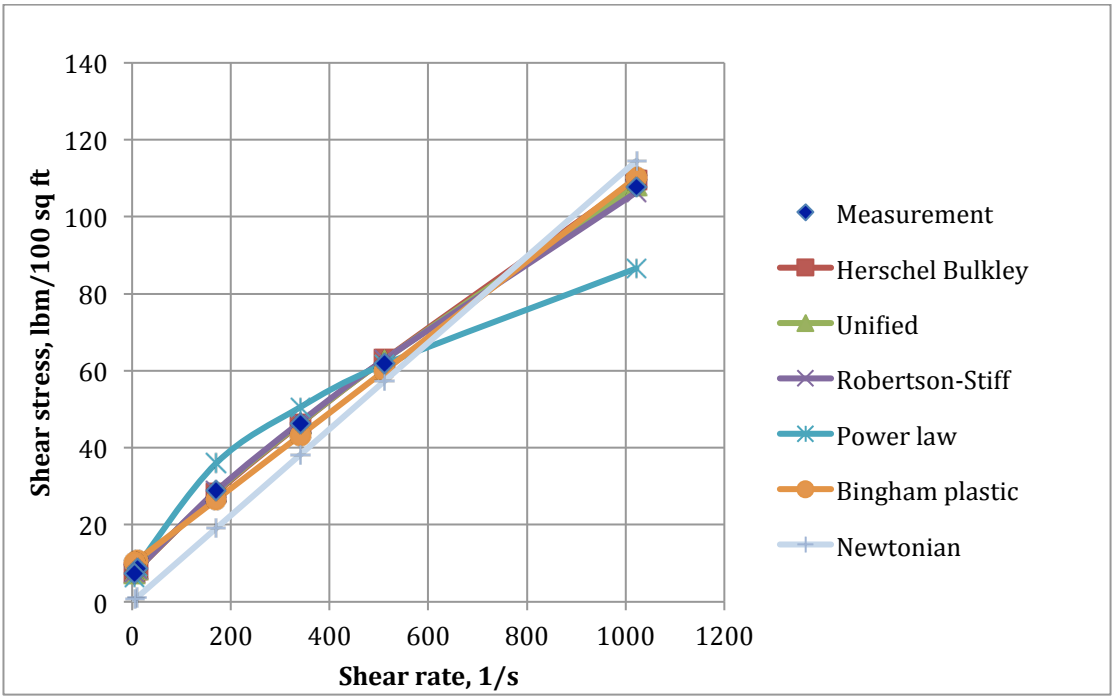

Figure 18: The different rheology models compared to measured data for the 70/30 OBM at room temperature.

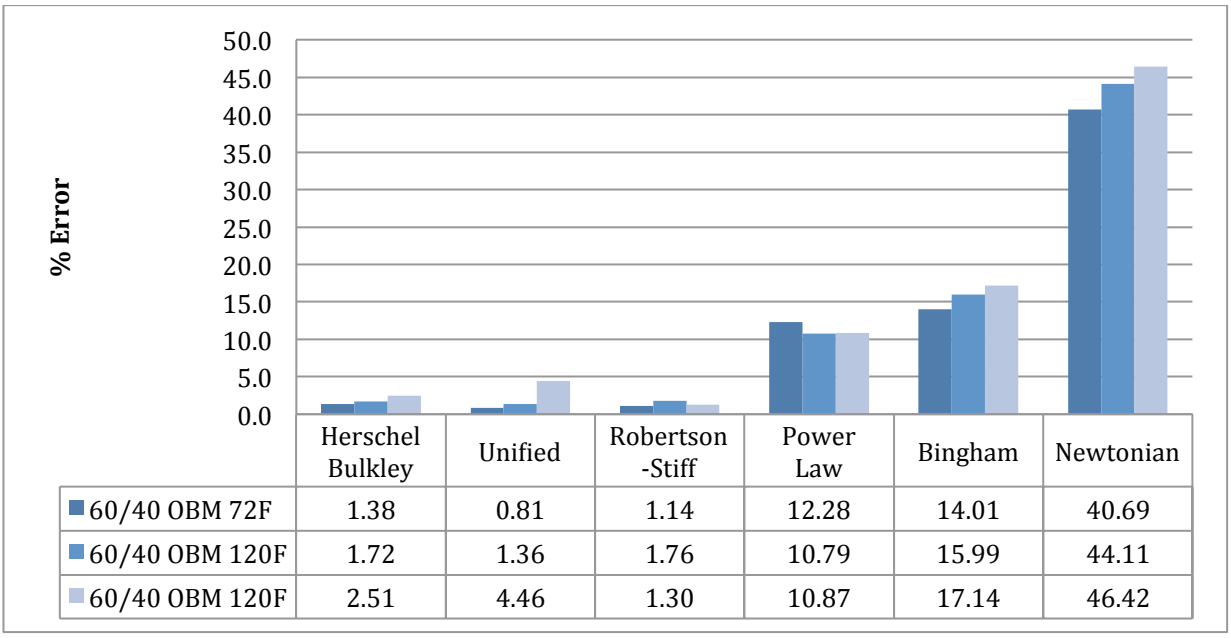

	Herschel Bulkley	Unified	Robertson -Stiff	Power Law	Bingham	Newtonian
60/40 OBM 72F	1.38	0.81	1.14	12.28	14.01	40.69
60/40 OBM 120F	1.72	1.36	1.76	10.79	15.99	44.11
60/40 OBM 120F	2.51	4.46	1.30	10.87	17.14	46.42

Figure 19: The error of the rheology models compared for the 70/30 OBM at 72, 120 and 180°F.

Similar to the 60/40 OBM, the error ranges shows best result for Herschel Bulkley, Unified and Robertson-Stiff. The overall performance in terms of % error for all temperature phases is best represented by Robertson-Stiff, considering the small spike in % error shown by the Unified model at 120°F.

Power Law and Bingham are showing higher % error in this mud system as well, and an even higher error with the Newtonian model.

4.2.3. Rheology Modelling and Analysis of 80/20 OBM

The different rheology models of the OBM with an oil-water ratio (OWR) of 80/20 at room temperature of 72°F is shown in Figure 20.

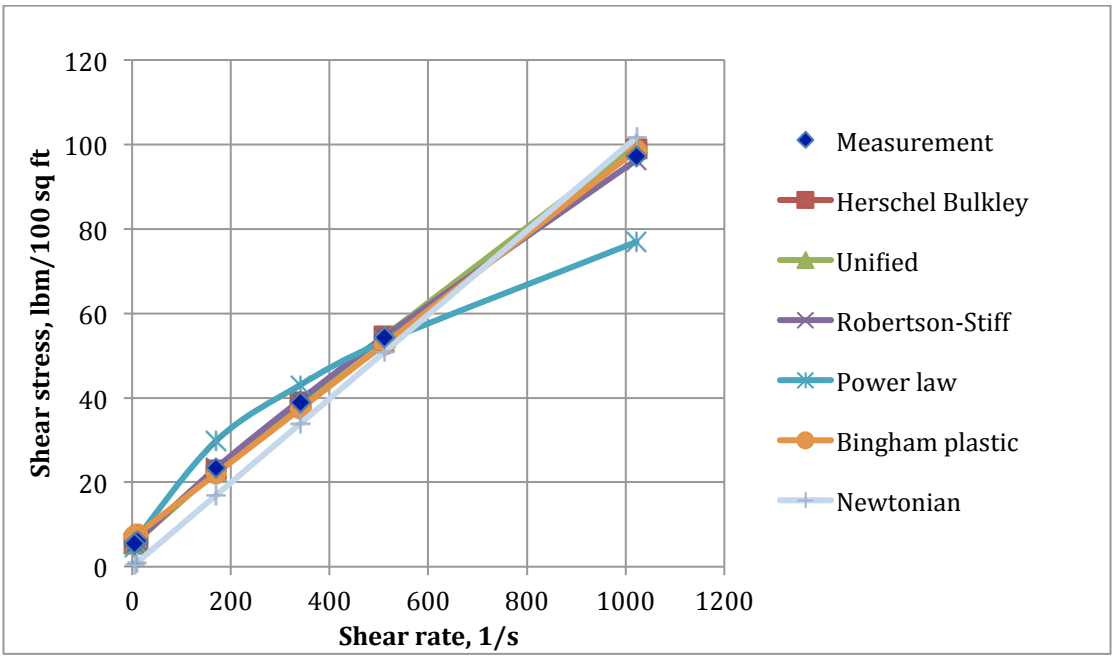

Figure 20: The different rheology models compared to measured data for the 80/20 OBM at room temperature.

It is seen that the Robertson-Stiff has the best overall performance at all temperature phases for the 80/20 OBM as well. A spike in % error for the Unified model at 120°F is observed in this case as well, similar to the 70/30 OBM.

Again, the Power Law and Bingham have an elevated % error, and the same with the Newtonian. These three models are poor models to be considered for the 80/20 OBM.

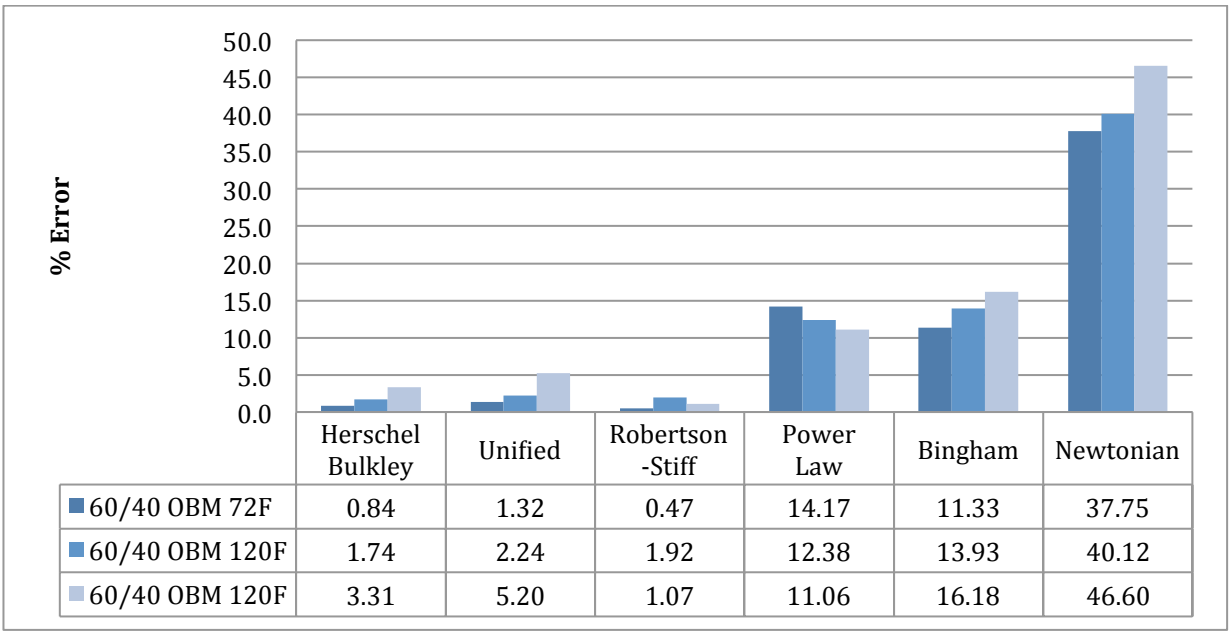

	Herschel Bulkley	Unified	Robertson -Stiff	Power Law	Bingham	Newtonian
60/40 OBM 72F	0.84	1.32	0.47	14.17	11.33	37.75
60/40 OBM 120F	1.74	2.24	1.92	12.38	13.93	40.12
60/40 OBM 120F	3.31	5.20	1.07	11.06	16.18	46.60

Figure 21: The error of the rheology models compared for the 80/20 OBM at 72, 120 and 180°F.

4.2.4. Rheology Modelling and Analysis of 90/10 OBM

The different rheology models of the OBM with an oil-water ratio (OWR) of 90/10 at room temperature of 72°F is shown in Figure 22.

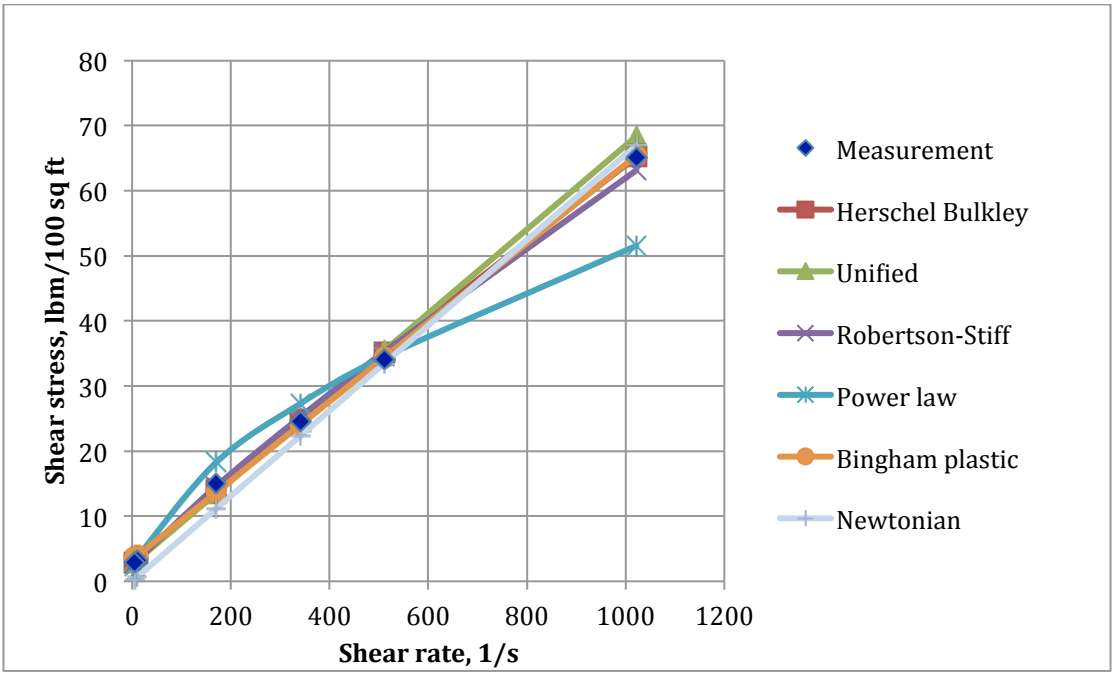

Figure 22: The different rheology models compared to measured data for the 90/10 OBM at room temperature.

For the 90/10 OBM, the Herschel Bulkley-, Unified- and Robertson-Stiff-models gives the best results. IT is interesting to see that the lowest error is obtained for all of these three models at 120°F.

As with the previous three OBMs presented, the Power Law, Bingam and Newtonian models are poor models for these mud systems.

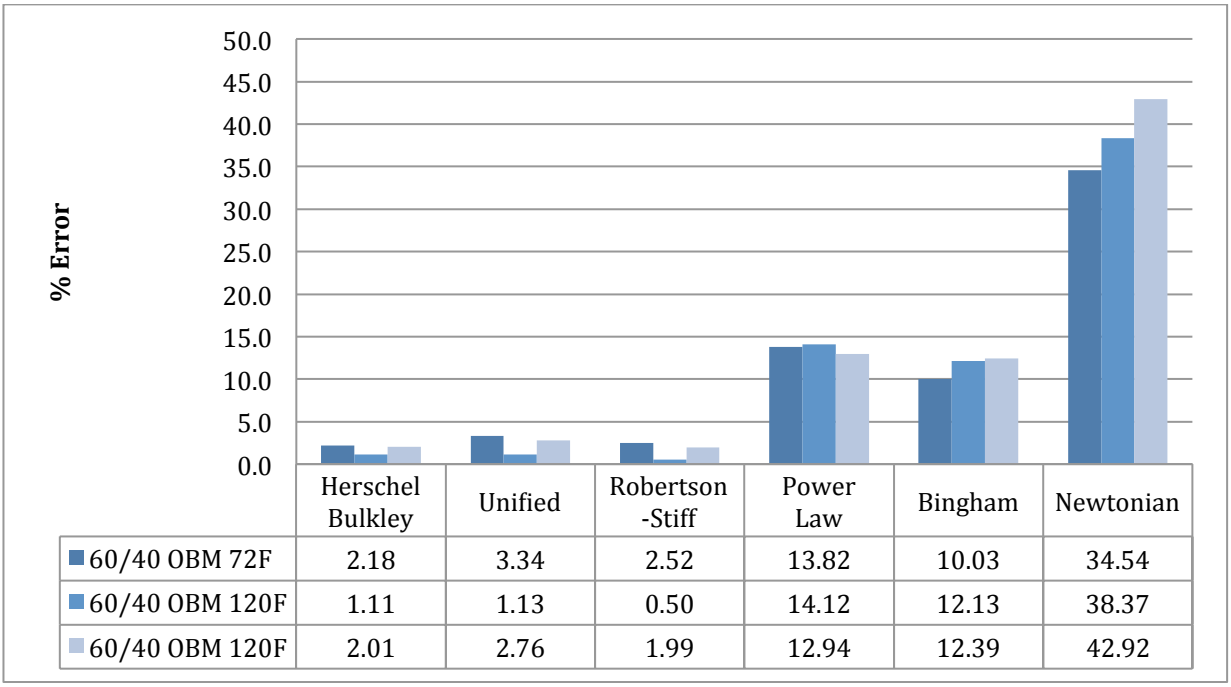

	Herschel Bulkley	Unified	Robertson -Stiff	Power Law	Bingham	Newtonian
60/40 OBM 72F	2.18	3.34	2.52	13.82	10.03	34.54
60/40 OBM 120F	1.11	1.13	0.50	14.12	12.13	38.37
60/40 OBM 120F	2.01	2.76	1.99	12.94	12.39	42.92

Figure 23: The error of the rheology models compared for the 90/10 OBM at 72, 120 and 180°F.

4.2.5. Temperature dependant plastic viscosity modelling of the four mud systems

In order to generate a correlation equation for the plastic viscosity with varying temperature, the rheological data from the experimental tests were analysed and plotted in Figure 24.

The plastic viscosity is calculated from the equations described for the Bingham-model in Section 2.7.2.1.

It is observed that the plastic viscosity of the 60/40 OBM is influenced greatly by temperature variations, when comparing with the other mud systems. This also indicates that the 60/40 OBM will show more variation in cuttings transport efficiency at different temperatures.

The three remaining mud systems have a much lower decline in plastic viscosity as temperature is increased.

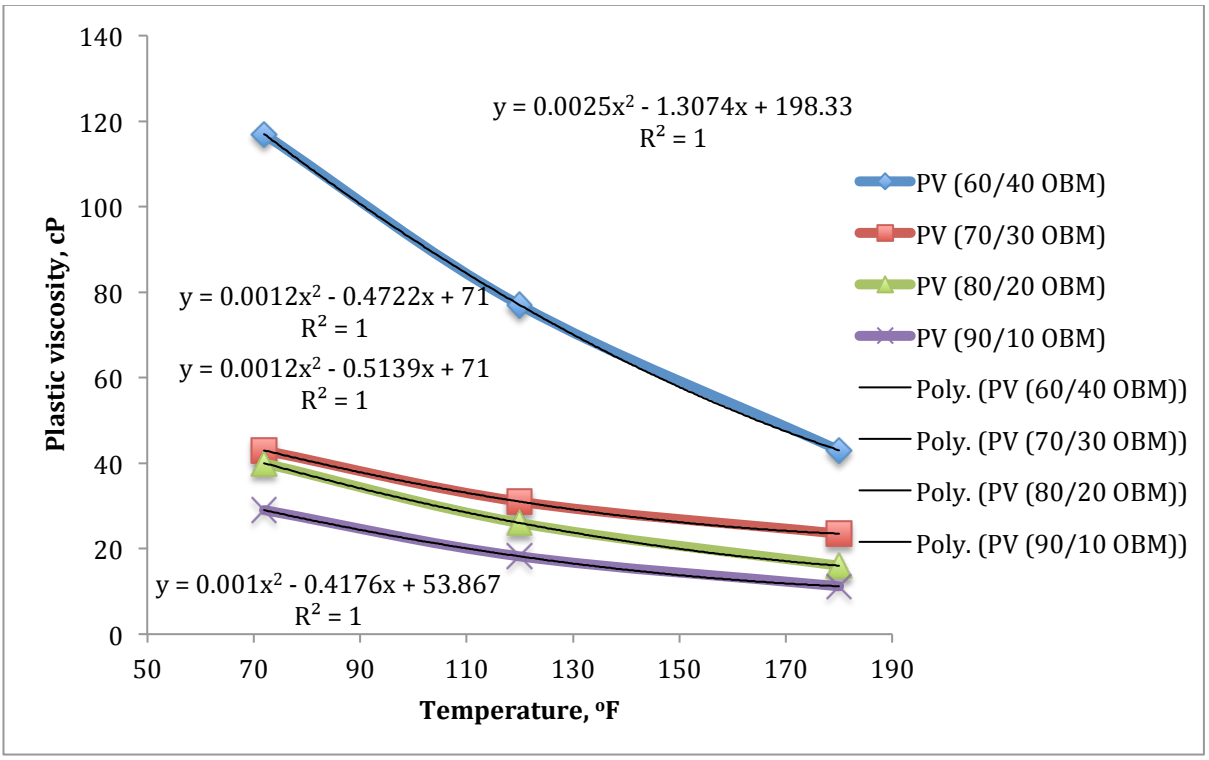

Figure 24: Comparison of the effect of temperature on the plastic viscosity of the OBMs.

The equations for calculating the plastic viscosity in the temperature range of 72-180°F are presented in Table 3.

Table 3: Plastic viscosity models that are temperature dependent.

Mud system	Plastic Viscosity Equation	R^2
60/40 OBM	$PV = 0.0025T^2 - 1.3074T + 198.33$	1
70/30 OBM	$PV = 0.0012T^2 - 0.4722T + 71$	1
80/20 OBM	$PV = 0.0012T^2 - 0.5139T + 71$	1
90/10 OBM	$PV = 0.001T^2 - 0.4176T + 53.867$	1

4.2.6. Temperature dependant yield stress modelling of the four mud systems

The equations for correlation of the yield stress at various temperatures are also generated. The polynomial trendline is the best fit for the measured data, as shown in Figure 25.

The yield stress is calculated from the equations described for the Bingham-model in Section 2.7.2.1.

Both the 70/30 and 90/10 OBMs have a minor increase in yield stress as the temperature is increased. On the other hand, the 60/40 and 80/20 OBMs reaches a minimum point at 120°F. These two OBMs also has a slight increase to a point below the original 72°F value when temperature is increased further to 180°F.

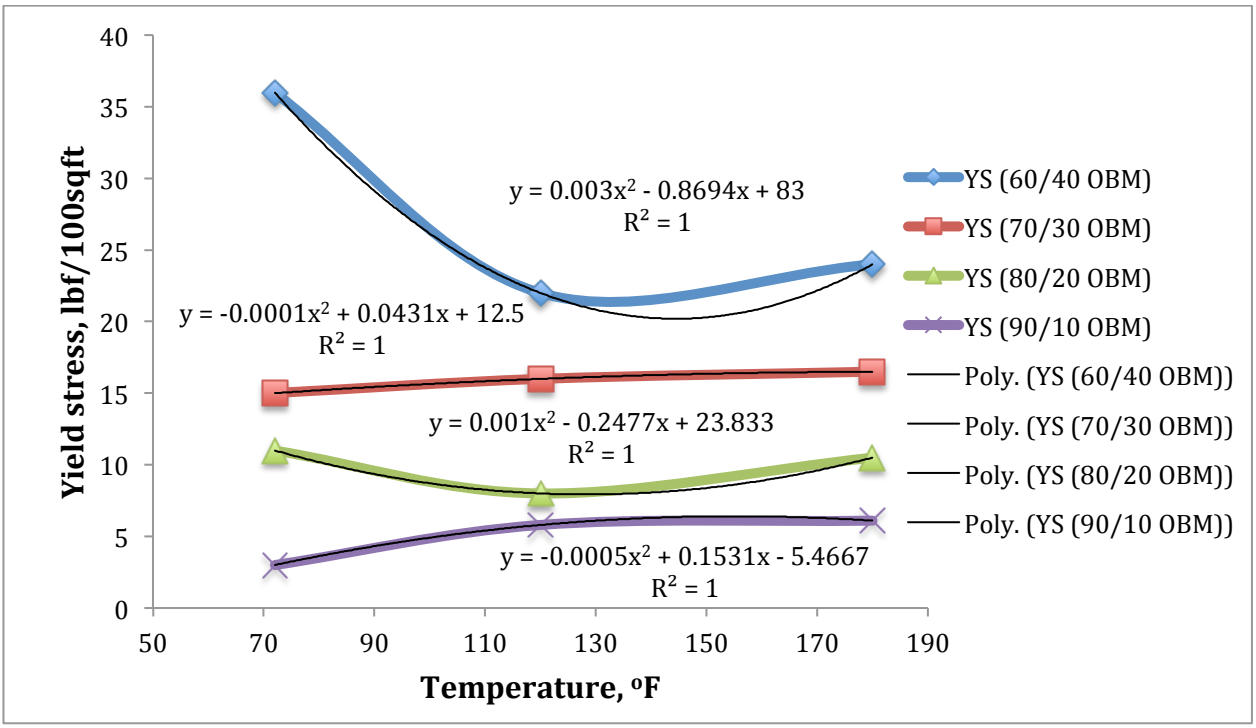

Figure 25: Comparison of the effect of temperature on the yield stress of the OBMs.

The equations for yield stress as a function of temperature (in the range of 72-180°F) is presented in Table 4.

Table 4: Yield stress models that are temperature dependent.

Mud system	Plastic Viscosity Equation	R^2
60/40 OBM	$YS = 0.003T^2 - 0.8694T + 83$	1
70/30 OBM	$YS = -0.0001T^2 + 0.0431T + 12.5$	1
80/20 OBM	$YS = 0.001T^2 - 0.2477T + 23.833$	1
90/10 OBM	$YS = -0.0005T^2 + 0.1531T - 5.4667$	1

4.3. Hole cleaning efficiency of the mud systems

The mud systems will be analysed in order to see how they perform during hole cleaning. The comparisons will be performed at a temperature of 72°F, since all fluid parameters are known at this temperature. The rheological parameters are presented in section 4.1.

The efficiency of cuttings transport is an important part in maintaining effective hole cleaning during a drilling operation. There are several parameters that impact the cuttings transport efficiency, which are the properties of the fluid and cutting as well as the operational parameters (Abimbola et al., 2014).

4.3.1. Simulation setup

In order to simulate the cuttings transport, the software Well-Plan by Landmark was used. To perform the simulation, a rheology model had to be chosen, which was the Power Law model in this thesis. The cuttings-, well- and operational parameters are assumed constant for the simulations performed.

The experimental well used for the simulation is 11003.3 ft. long in measured depth. As illustrated in Figure 26, the constructed well consists of a 13 3/8 in. casing followed by a 12.250 in. open hole. The drill string consists of a 5 in. drill pipe and a bottom hole assembly (BHA). The full details of the well and the parts can be found in Appendix B. The well inclination for the simulated well can be seen in Figure 27.

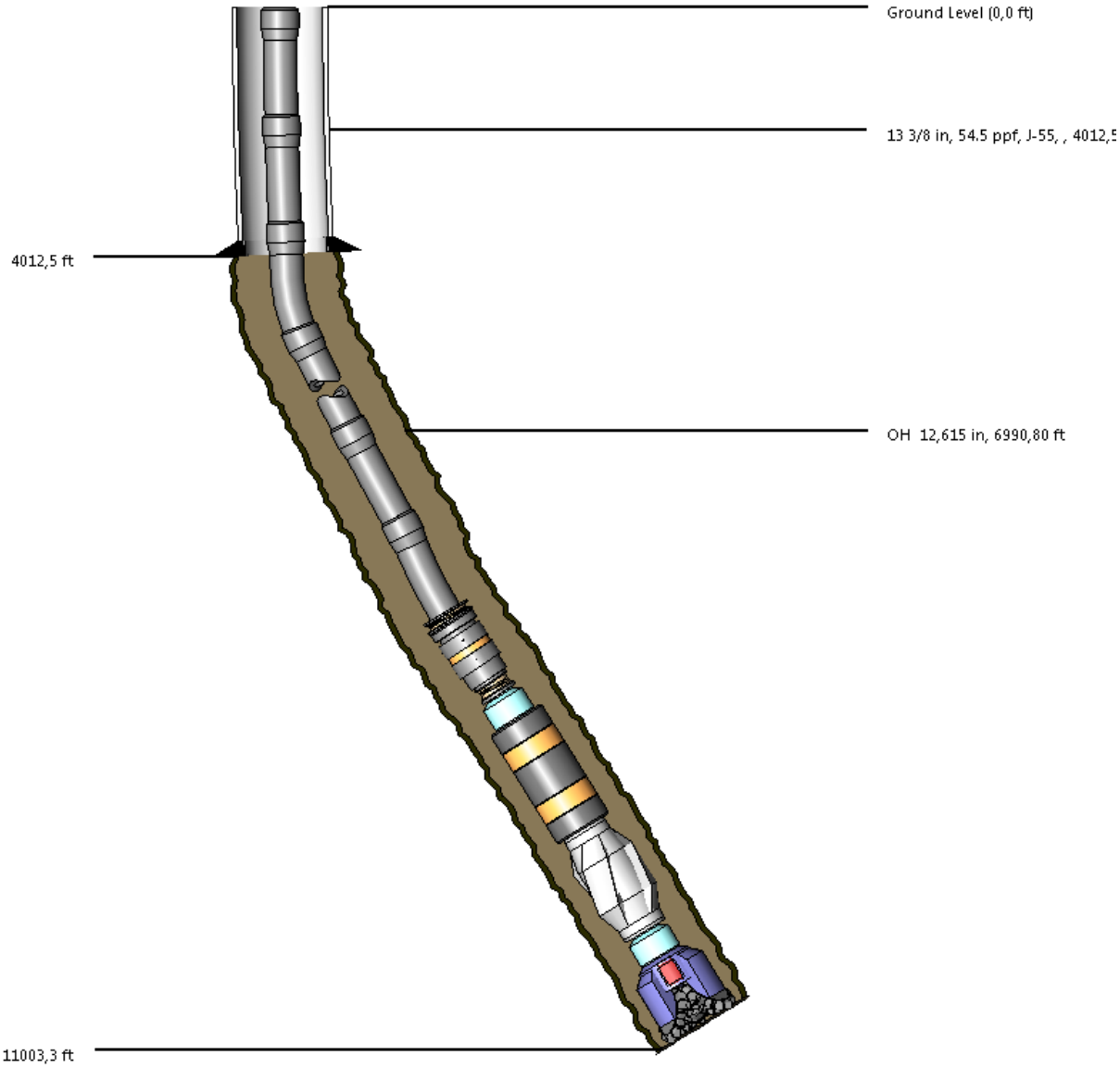

Figure 26: Experimental well used for simulation.

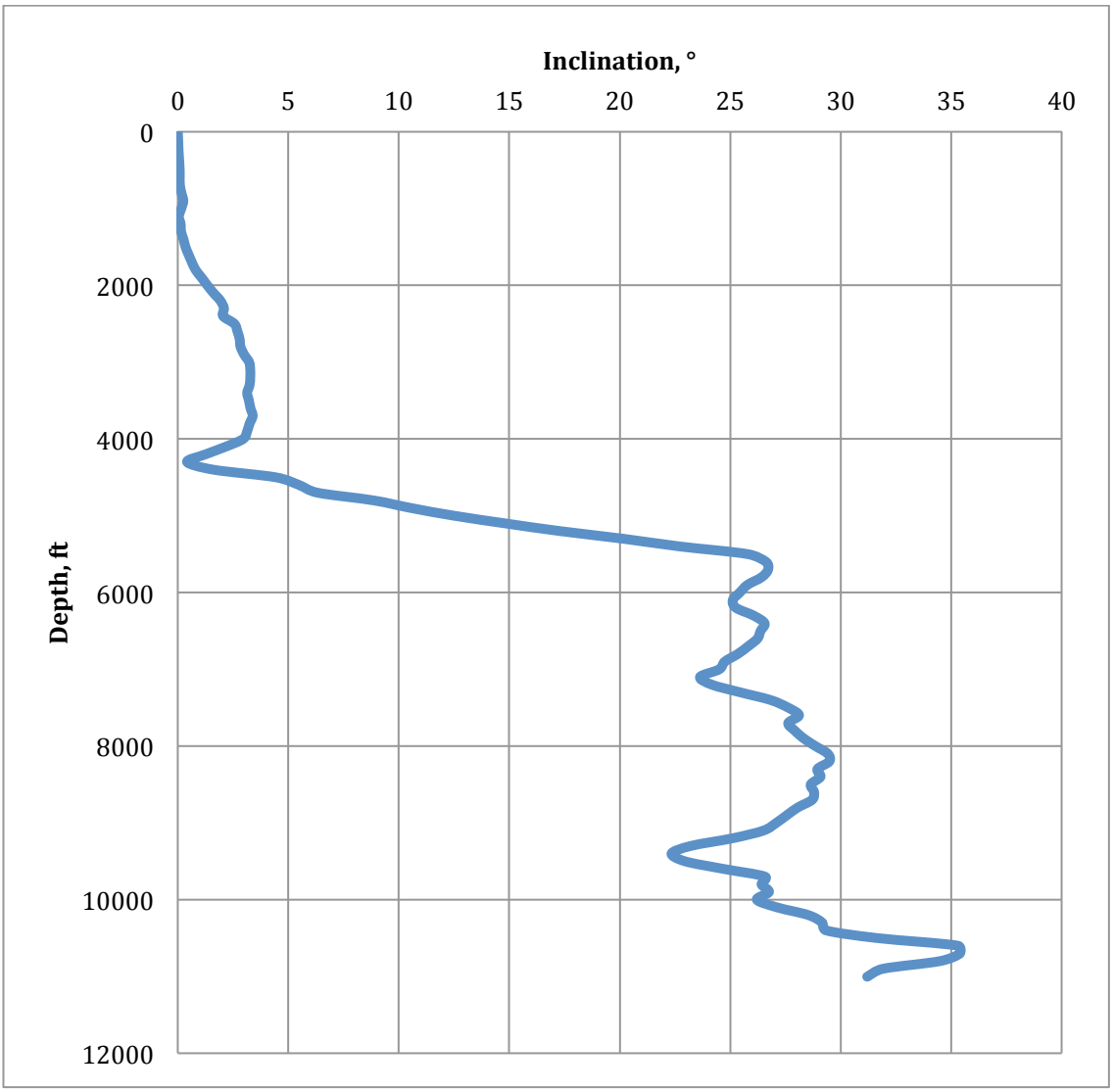

Figure 27: Well inclination versus depth.

4.3.2. Minimum flow rate simulation

The minimum flow rate can be defined as a critical velocity required to remove or to prevent accumulations of cuttings during a drilling operation. In this experimental well, the performance of the four mud systems was simulated with respect to minimum flow rate as a function of well inclination. The input data used are shown in Table 5. The flow rates acquired here represents a well with a uniform 5" drill string without BHA.

Table 5: Transport analysis data for minimum flow rate simulation.

Cuttings diameter (in)	0.125
Cuttings density (s.g)	2.500
Bed porosity (%)	36.00
Rate of penetration (ft/hr)	60.0
Rotary speed (rpm)	100
Bit diameter (in)	8.500
Annulus diameter (in)	8.500
Pipe diameter (in)	5.000
Joint diameter (in)	5.500
Mimumum pump rate (gpm)	100.0
Increment pump rate (gpm)	200.0
Maximum pump rate (gpm)	800.0

The simulated results are presented in Figure 28. As can be seen from the simulated results, the 60/40 OBM requires a lower flow rate when the hole angle is increased, compared to the other mud systems.

For the three other mud systems, the well inclination can be divided into two regions:

- Region 1 (0-45°)
- Region 2 (45-90°)

During region 1, the 90/10 OBM has the highest minimum flow rate, and a lower minimum flow rate is observed for the 80/20 and 70/30 OBMs. However, during the transition to region 2, the 90/10 and 80/20 OBMs have an equal minimum flow rate. As the 80/20 OBM flow rate increases significantly as a function of inclination, the 90/10 OBM has a slight increase and is equal to the 70/30 OBM when an inclination of 90° is reached. It should be noted that these results are valid for the well parameters used during the simulation.

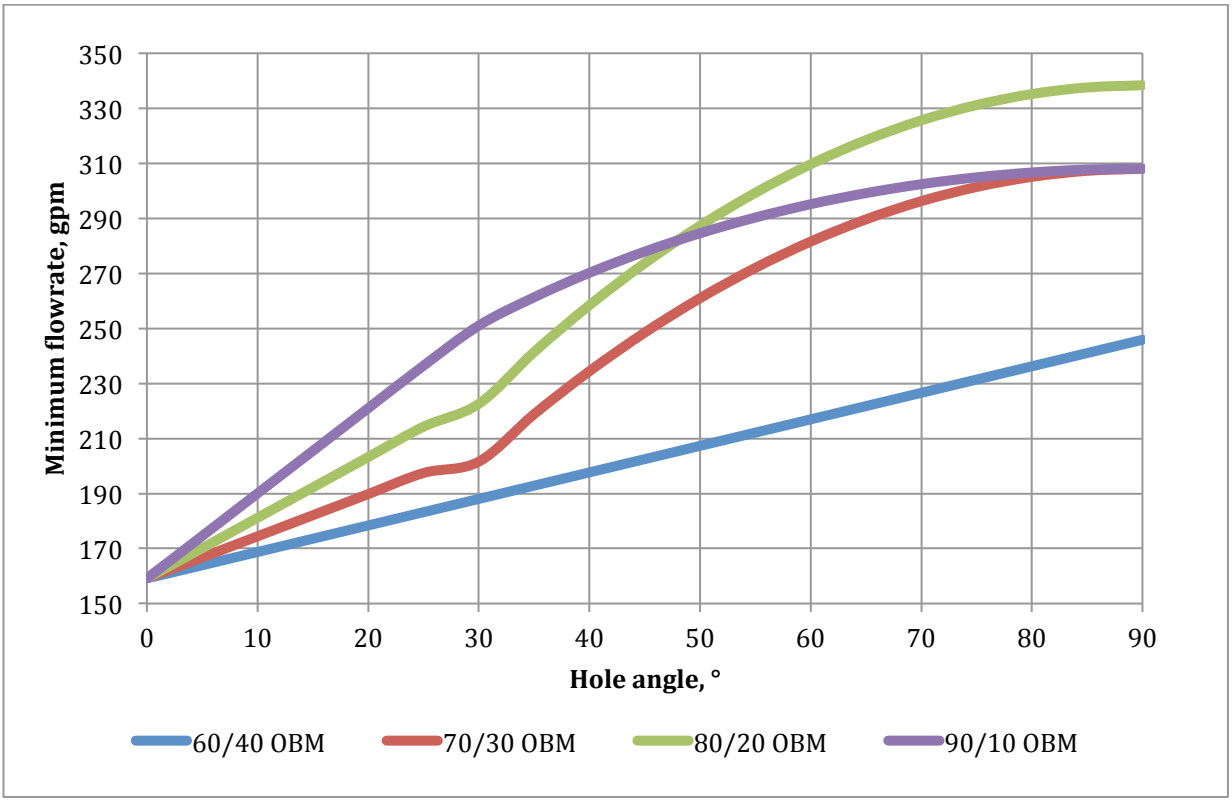

Figure 28: Minimum flow rate simulation results.

4.3.3. Bed height simulation results and analysis

The carrying capacity of cuttings for the four mud systems will be analysed by looking at the height of the bed deposit. The bed height is the deposited cuttings that accumulate on the bottom of the well, and a high bed height can be the result of poor hole cleaning. Poor hole cleaning also causes undesired operational effects during a drilling operation, such as high torque, excessive drag on the drill string, stuck pipe and well control problems (Gulsrud et al., 2009).

Sifferman et al. (1974) performed studies on various drilling fluids, and the results showed that the cuttings transport efficiency increased with an increase of fluid viscosity for oil systems.

Okrajni and Azar (1986) investigated several inclination regions for water based mud, and found that under laminar flow, a higher yield value of the mud reduces the concentrations of cuttings.

The drilling fluid was circulated with a rate of 400 gpm during the simulation, which was determined from the minimum flow rate simulation results shown in Table 6.

Table 6: Minimum flow rate for the mud systems.

OBM	60/40	70/30	80/20	90/10
Minimum flow rate (gpm)	440.4	457.1	505.4	546.3

During the simulation of bed height, the parameters presented in Table 7 were used. The minimum flow rate was re-simulated for all four mud systems by using these parameters and the experimental well data presented in Appendix B. The flow regime in the annulus has been determined as laminar, from the calculated data presented in Appendix C.

Table 7: Transport analysis data for bed height simulation.

Rate of penetration (ft/hr)	Rotary speed (rpm)	Pump rate (gpm)	Cuttings diameter (in)	Cuttings density (s.g)	Bed porosity (%)	MD calculation interval (ft)
60.0	100.0	400.0	0.125	2.50	36.00	100.0

The results from the cuttings transport simulation are shown in Figure 29. When comparing the mud systems in terms of bed height, it is seen that the 60/40 mud system has the best performance, while the 90/10 has the poorest performance. The difference of these two systems at maximum bed height is 2.5 inches. This is the expected performance, when looking at the minimum flow rates generated for the simulated scenario.

Considering the laminar flow regime, it is seen that an increase in YS as well as viscosity causes a better hole cleaning performance for these four OBMs, as previous studies indicate.

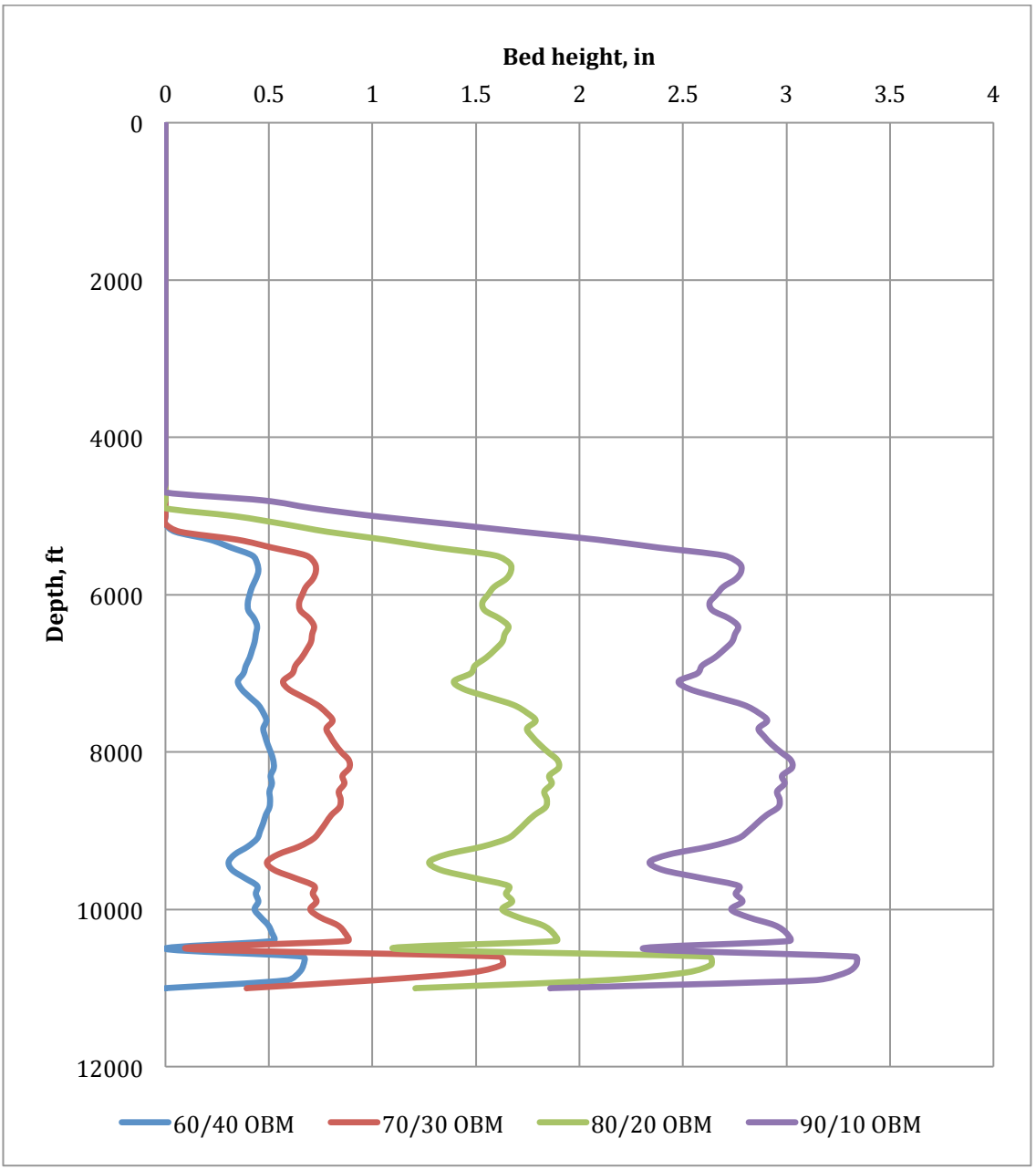

Figure 29: Comparison of the bed height between the four mud systems.

When analysing the cutting bed profile with the well inclination, it is seen that the profile exhibit a similar trend for all of the four mud systems. This trend is expected, considering that there is no bed deposit in the vertical section of the well. The bed height also starts to build quickly as the inclination has a steep increase at 4300 ft.

4.4. Bridging test results

In the experiments, 4.5 gram of LC-lube was mixed with 200 gram of the OBMs, which gives a concentration of 13.82 pounds per barrel (ppb) of LC-lube. The observations from the results will be discussed below. As mentioned previously, the experiments were conducted with slot openings of 250, 300, 400 and 500 microns.

4.4.1. Experimental test with 60/40 OBM

From the experimental data, it can be seen that the 250 and 300 micron slot openings are increasing at a similar rate. The 250 micron is able to create a stable bridge that withstand a higher pressure than the 300 micron during the first four minutes. Afterwards, it can be seen that the 300 micron is surpassing the 250 micron, meaning that it is able to create a bridge that can resist a higher pressure before collapsing. Both of these openings are either at or below the D50 of the PSD.

When looking at the two openings that are higher than the D50, the 400 and 500 microns, it can be seen that they are not able to build up as high pressure as the two other openings during the tests. Considering that the slot openings are larger than the D50, it is very possible that a lot of the particles pass through the opening, unless the particles of a size higher than the opening are able to start forming a bridge. By following this logic, it would make sense that the 400 micron opening is showing better results than the 500 micron.

As the bridge collapses for the 400 micron, there will still be fragments of the bridge left as a new bridge is forming, preventing a pressure drop down to 0 MPa. For the 500 micron it appears that as the bridge collapses, a new bridge will have to be created from scratch. This trend can be seen from the Figure 30, where pressure is dropped down to 0 MPa for the 500 micron opening. This can be explained from the fact that there will only be roughly 10% particles that are of a size larger than the fracture opening of 500 micron, since the D90 for the LC-lube mixture is 500 micron.

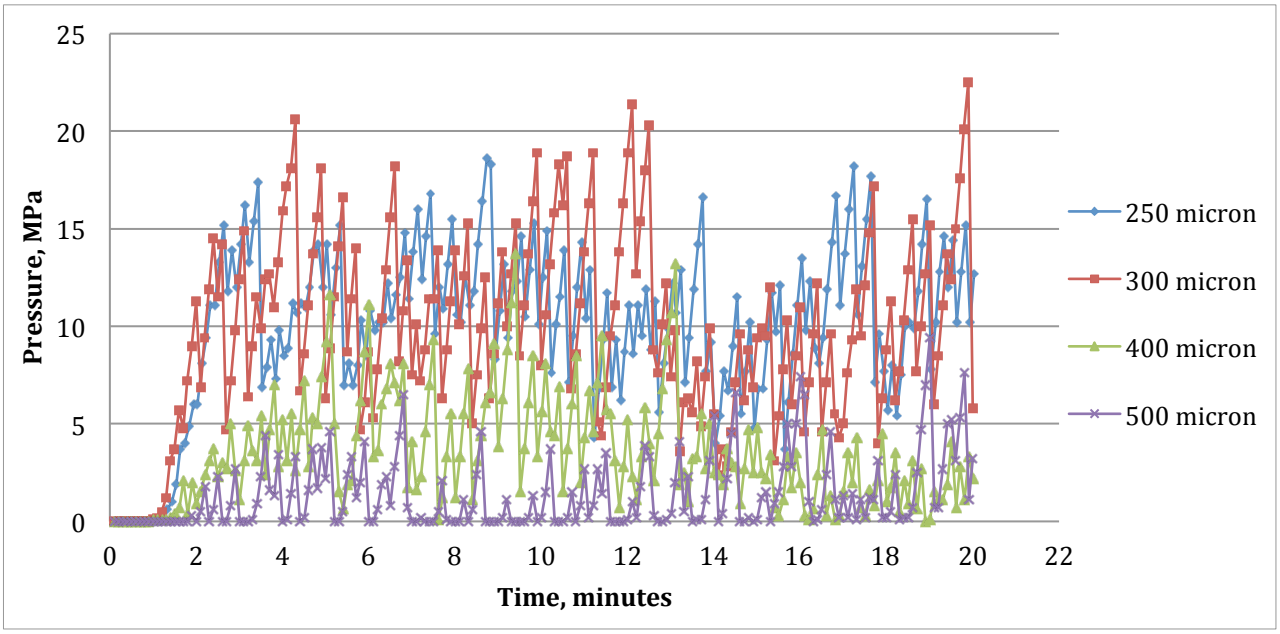

Figure 30: Experimental pressure data from the lost circulation tests with the 60/40 OBM.

4.4.2. Experimental test with 70/30 OBM

For the 250 micron there is a high peak at the start of the experiment, when compared to the 300 micron that collapses during the initial build-up. However, afterwards in the experiments, the 300 micron is able to establish a better bridge in terms of resistance. While 300 micron falls off early, but builds up later, the opposite trend is seen for the 250 micron opening.

The best performance is as discussed shown for the 300 micron opening, which is closest to the D50 of the PSD. This opening is able to maintain the bridge and build up the resistance better than the 250 opening when looking at the overall performance.

The 400 micron opening has a slow build up of pressure resistance of the bridge, but performs relatively good when considering the increase of 100 micron at the opening, compared to the 300 micron. It is less probable that a bridge will start to form due to a less amount of the particles are this large.

For this specific mud system it is obvious from Figure 31 that the experiment shows much poorer data for the 500 micron opening in comparison to the other mud systems. It appears that in this case the system is not able to create a bridge until the 4 minute mark, and throughout the 20 minutes of experiments, the bridge does not reach its highest peak until the 16 minute mark.

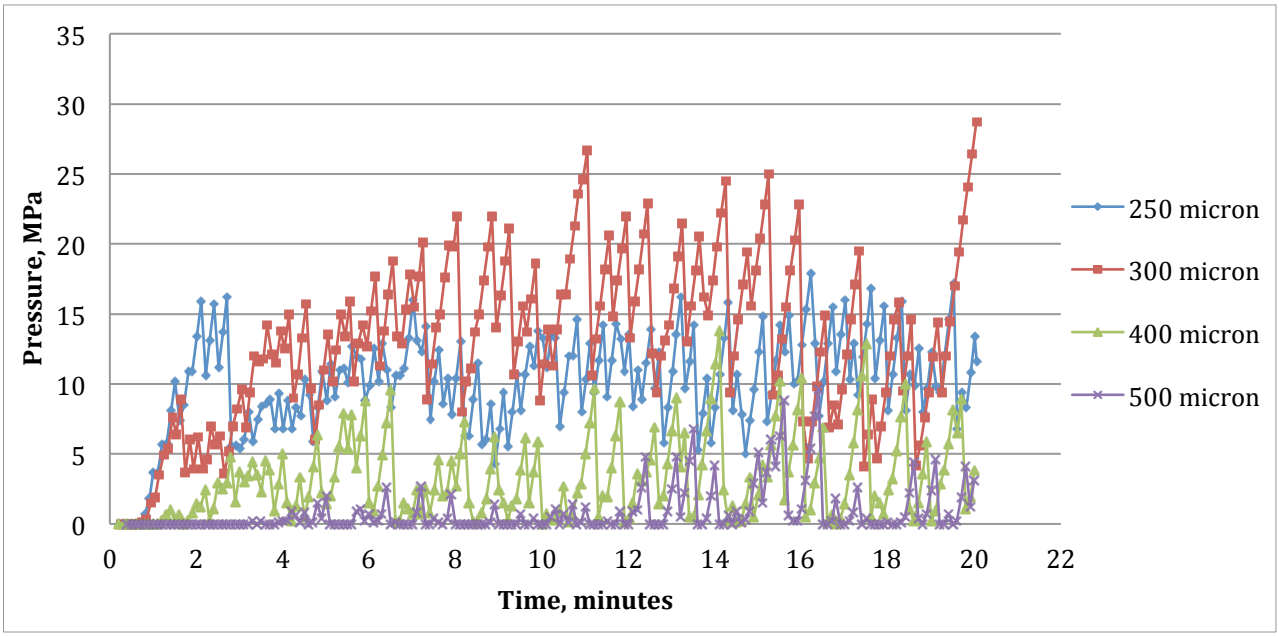

Figure 31: Experimental pressure data from the lost circulation tests with the 70/30 OBM.

4.4.3. Experimental test with 80/20 OBM

It is interesting to see that the 250 micron opening is able to achieve a higher pressure resistant bridge than the 300 micron opening for this mud system. During the first two minutes, the increase in rate is pretty consistent for the two openings. Although the 300 micron has an increased build-up later on, it is not able to reach the peaks of the 250 micron.

For this mud system, it also appears that the bottom pressure that is reached when the bridge collapses is much lower for the 300 micron opening. Considering the 50 micron difference between the openings, this might indicate that the 300 opening is not able to establish a stable bridge in this case, when comparing to the 300 micron opening for the 60/40 mud system.

The pressure build-up for the 400- and 500 micron openings occurs later than the two prior openings. During the middle and late stage of the experiment, both of the openings are able to produce a bridge that is able to withstand pressure in the range of 10-14 MPa (500 and 400 respectively).

The noticeable part with these larger widths for this mud system as well is the fragile nature of the bridges formed. Once the bridge for either of the widths collapse due to a high pressure, it appears that most of the bridge will have to be rebuilt again. This observation is based upon the pressure readings, where the pressure is seen to decline to zero for these openings.

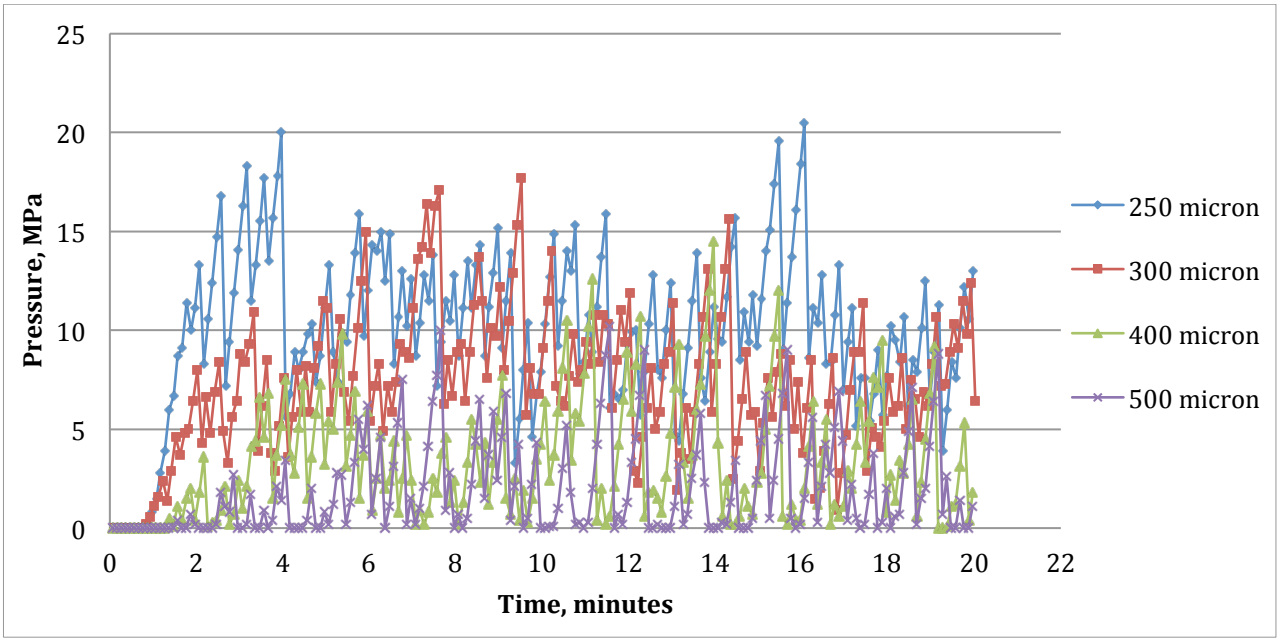

Figure 32: Experimental pressure data from the lost circulation tests with the 80/20 OBM.

4.4.4. Experimental test with 90/10 OBM

Similar to the 80/20 mud system, the 250 micron opening shows a significant increase in what pressure the bridge is able to withstand, when compared to the 300 micron opening. The rate at the start for these two openings is near identical during the first build-up, but start to deviate at the 4-minute mark.

It is observed that the bridge created by the 250 slot opening for this mud system surpasses all of the other mud systems by far, with the highest peak at 42 MPa. When the bridge collapses for the 250 micron opening, the pressure does not drop down to the same level that the 300 micron opening drops to during bridge collapse. This appears to allow the bridge to start building up again with a more particles left from the former bridge.

The 400 and 500 micron opening has a very slow rate, where the bridges do not appear to form till after the 2-minute mark. The resistance of these bridges are fragile, as seen in the prior mud systems, where the pressure achieved before collapse is low.

It should also be noted that both of these larger slot openings leads to a pressure drop down to 0, although the 400 micron opening is better at maintaining the bridge remnants when it collapses. The highest pressure achieved for these two openings are in the range 9.5-12 MPa (400 micron and 500 micron respectively), which shows that the larger opening is actually able to resist a higher pressure. The uniformity of the particles distributed in the mud may have affected this outcome.

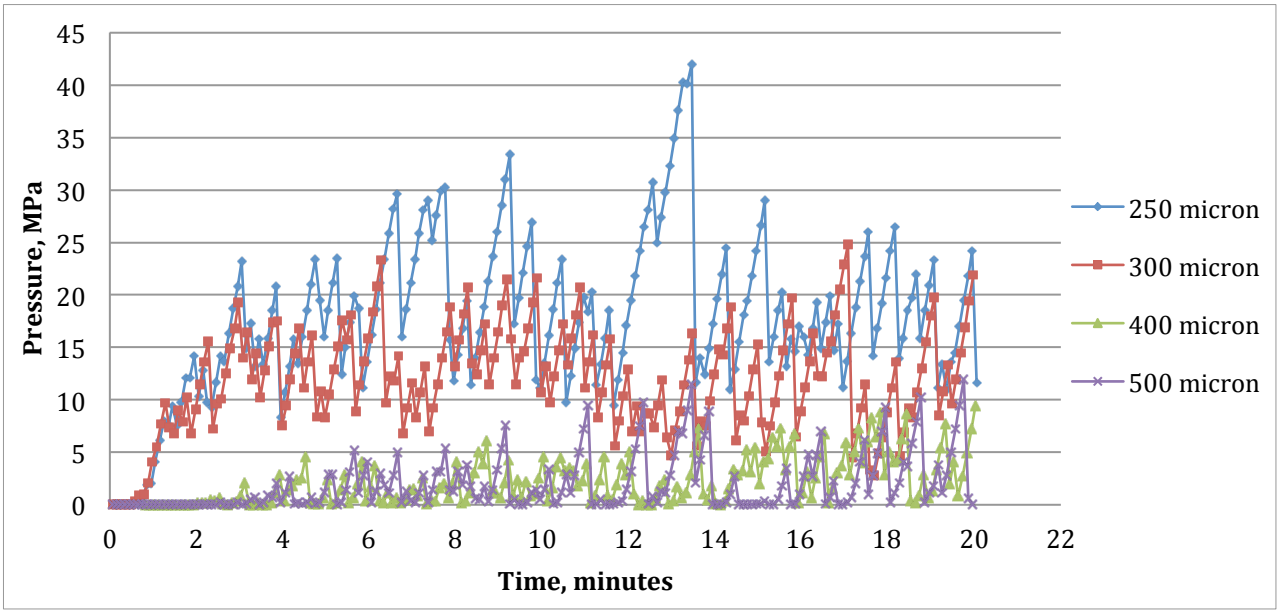

Figure 33: Experimental pressure data from the lost circulation tests with the 90/10 OBM.

4.5. Comparison of experimental data from tests with 60/40, 70/30, 80/20 and 90/10 mud systems

In the following subsections the bridging and pressure variations will be compared for the different mud systems, when the slot opening is the same. Important parameters will be discussed in further detail in later sections; therefore observations from the pressure plots will be mentioned below.

4.5.1. Comparison of the mud systems at 250 micron slot opening

The initial rate is similar for all mud systems but the 60/40, which occurs a bit later. An increased pressure due to the forming of bridges happens for all of the muds systems, but it collapses after a while. Afterwards the bridge seems to maintain its core, but collapses and then rebuilds throughout the experiments.

It is very clear that the 90/10 OBM performs better than any of the other mud systems, as mentioned earlier. The best bridge formed for this OBM is able to resist a pressure which is twice as high of what the other OBMs could resist.

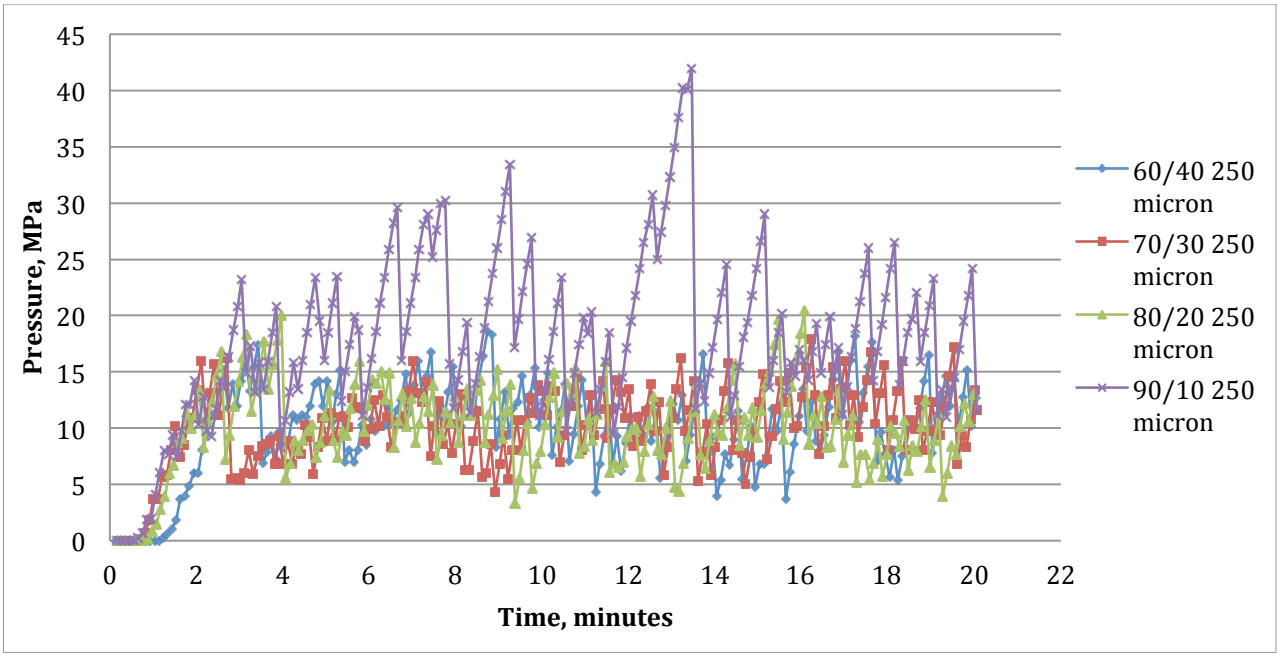

Figure 34: Experimental pressure data from the lost circulation tests with a 250 micron slot opening for the four OBMs.

4.5.2. Comparison of the mud systems at 300 micron slot opening

As seen for the 250 micron opening, the initial rate kicks off before the 2-minute mark. The 60/40 and 90/10 OBMs have a similar trend throughout the experiment. The bridge seems to be able to stay more intact for the 90/10 OBM though, since the pressure drops are more frequent and larger for the 60/40 OBM.

The 80/20 OBM appears to struggle with creating a resistant and good bridge compared to the other OBMs, as seen by the low-pressure readings during the experiment.

Although the 70/30 OBM has a collapse during the initial rate, it appears to be able to recreate bridges that are able to withstand higher pressure than the other OBMs. A lower pressure drop during collapse of bridges is also observed for this mud.

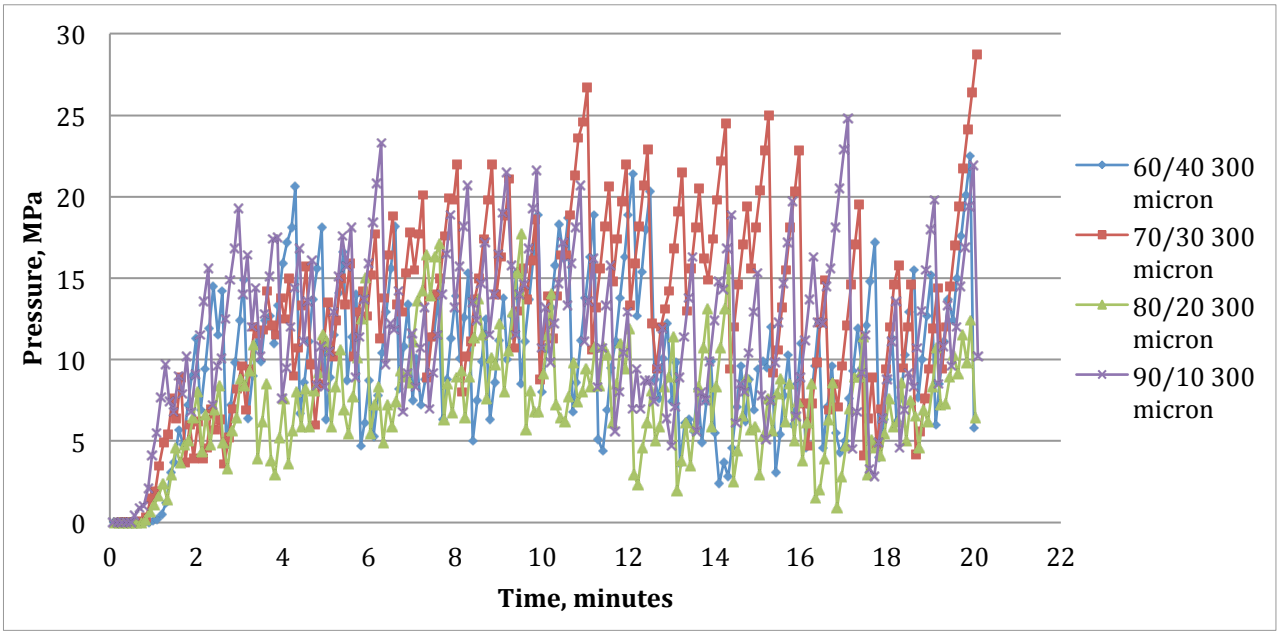

Figure 35: Experimental pressure data from the lost circulation tests with a 300 micron slot opening for the four OBMs.

4.5.3. Comparison of the mud systems at 400 micron slot opening

The initial rate occurs much slower for the 400 micron opening than the smaller openings, and is not able to quickly achieve a pressure resistant bridge. The rate is most likely slow in this case due to the increased opening width.

It is observed that the three OBMs with the lesser OWR act similar and are able to create the best bridges. The 90/10 OBM is acting poorly, and it is seen that the pressure drops to zero throughout the experiment.

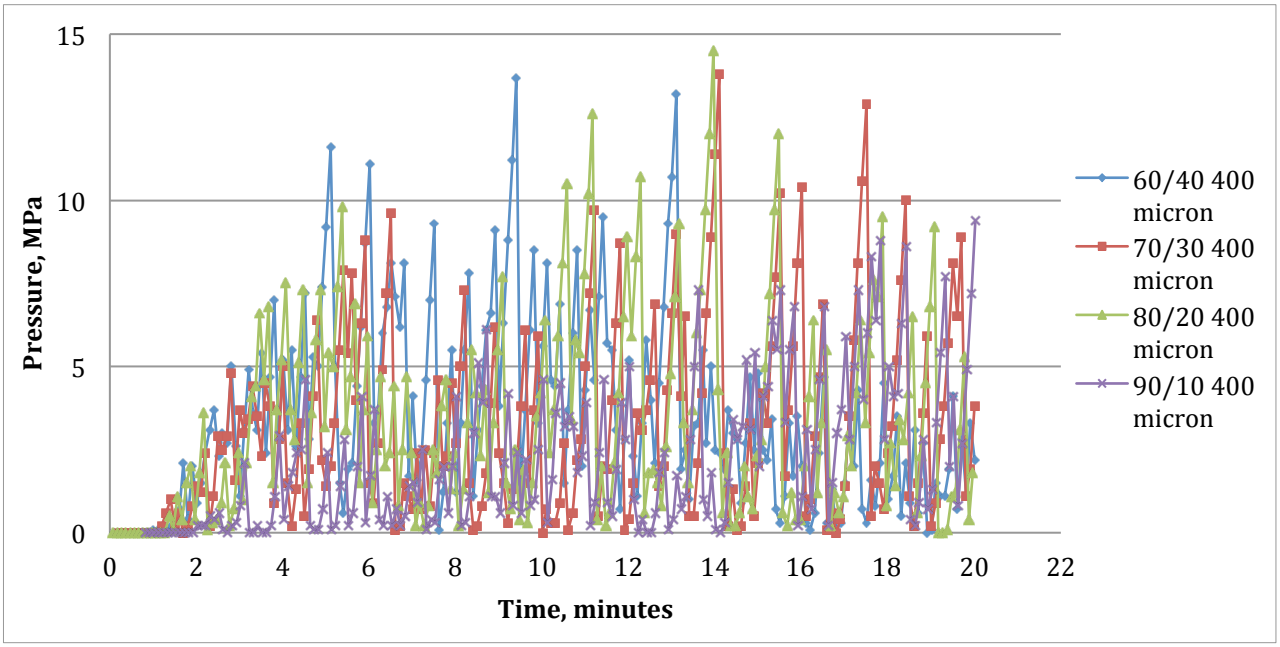

Figure 36: Experimental pressure data from the lost circulation tests with a 400 micron slot opening for the four OBMs.

4.5.4. Comparison of the mud systems at 500 micron slot opening

The bridges formed during the 500 micron opening tests appears to be very fragile for all of the OBMs. Once a bridge is formed, it quickly collapses, and pressure is dropped to zero.

It is clear that the PSD used for the LC-lube is not able to create a bridge over this large fracture width. This can be expected when considering that the D90 of the mixture is 500 micron, meaning that only 10% of the particles are larger than the fracture width.

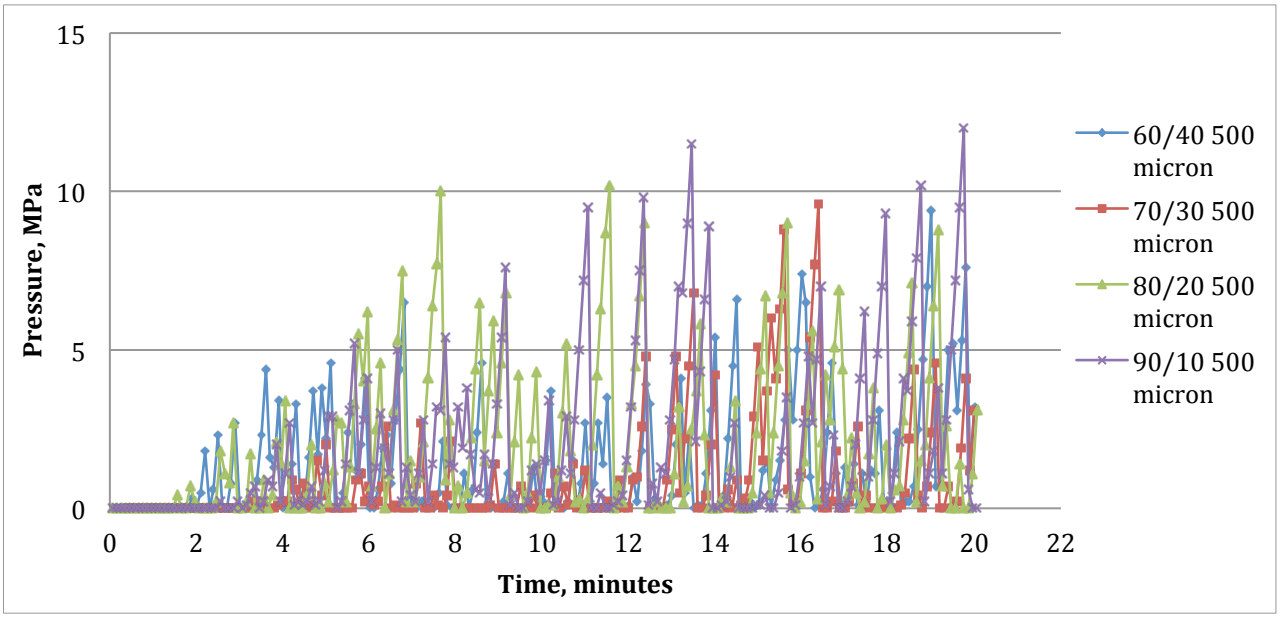

Figure 37: Experimental pressure data from the lost circulation tests with a 500 micron slot opening for the four OBMs.

4.6. Analysis of the results from lost circulation experiments

Earlier studies done by Toroqi (2012) on particle plugging during lost circulation tests led to a definition of parameters used in order to define the performance on the LCM. Some of these terms will be used in this thesis in order to evaluate the data obtained form the lost circulation experiments. The terms used will be explained briefly below.

Maximum pressure (P_{max}): The maximum pressure obtained during the experiment, which is influenced by the particle distribution as well as the uniformity of the fluid.

Average pressure (P_{avg}): The average pressure achieved during the experiment allows for a comparison of the mud samples, as it gives information about the average strength of the bridge.

Average peak pressure ($P_{P\text{-}avg}$): The average peak pressure is the average strength that the bridges are able to reach during the course of the experiment. This value denotes the differential pressure between the inside of the cylinder and the opening (atmospheric pressure).

Total number of peaks (N): Each peak that develops in the pressure plot during the test depicts a failed bridge that has been built. This means that the total amount of peaks will provide information about the ability to create a bridge for the combination of fluid and LCM.

The calculated values for the above parameters are listed in Table 8. In order to compare the different mud systems, the results will be plotted in graphs in the following sections, giving a better picture for the comparison.

Table 8: Calculated parameters from lost circulation tests with the four mud systems.

Mud system	Slot (micron)	Peaks (N)	$P_{P\text{-}avg}$ (MPa)	P_{avg} (MPa)	P_{max} (MPa)
60/40 OBM	250	57	13.06	10.06	18.6
	300	22	13.47	9.81	22.5
	400	54	5.49	3.51	13.7
	500	46	3.24	1.37	9.4
70/30 OBM	250	60	3.63	2.31	8.5
	300	27	16.44	11.10	28.7
	400	49	5.46	3.16	13.8
	500	41	2.36	0.86	9.6
80/20 OBM	250	54	13.04	10.06	20.5
	300	56	9.74	7.32	17.7
	400	54	5.41	3.34	14.5
	500	47	3.99	1.94	10.2
90/10 OBM	250	27	19.93	16.25	26
	300	46	15.55	11.98	26
	400	52	4.08	2.20	9.4
	500	44	4.04	1.96	12

4.6.1. Maximum pressure for the mud system

The maximum pressure obtained during the lost circulation experiments are shown in Figure 38. The four mud systems are gathered at the different slot openings in order to compare them side-by-side.

It can be seen that there is a decline in maximum pressure when the slot opening exceeds the D50 (310 microns) for the three OBMs with the lowest OWR. The 90/10 OBM has a slight increase from 400 micron to 500 micron, but this can be affected by the distribution of the particles as well as the degree of uniformity of the fluid inside the cylinder. The maximum pressure can therefore be varying and scattered to some extent.

Although the 90/10 shows the most promising results at 250 micron, the maximum pressure might have been different if an identical test had been run again for this system.

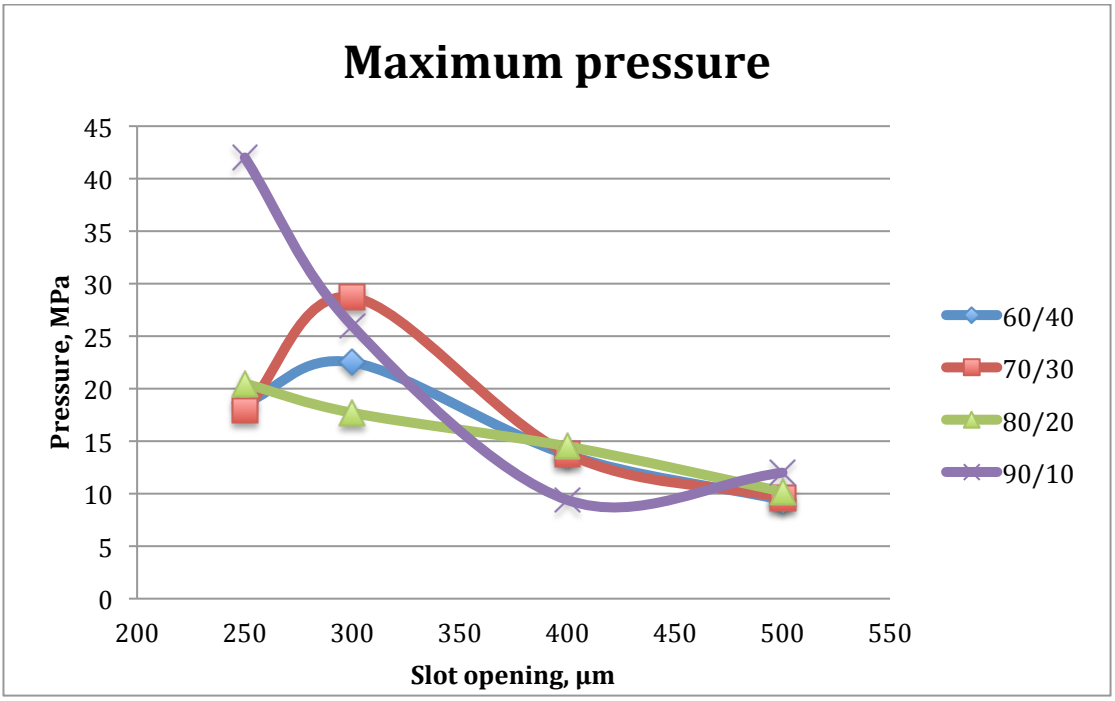

Figure 38: Data obtained for maximum pressure during lost circulation experiments.

4.6.2. Average pressure for the mud systems

The average pressure is near identical for the 60/40, 70/30 and 80/20 OBMs at 250 micron, which implies that the average strength of the bridge formed for these systems was the same. The 90/10 OBM shows variations, mostly due to the large spikes in maximum pressure during the experiment conducted.

Another observation as seen for the maximum pressure is the declination of pressure as the opening width is increased. The 90/10 OBM is considered the most promising at creating a bridge with the highest average strength for the two lowest opening widths.

While the 60/40 OBM has about the same average pressure when the slot opening is increasing from 250 micron to 300 micron, the 70/30 OBM has a slight increase. The

80/20 OBM decreases by about 2.5 MPa when the slot opening is increased to be closer to the D50 of the PSD.

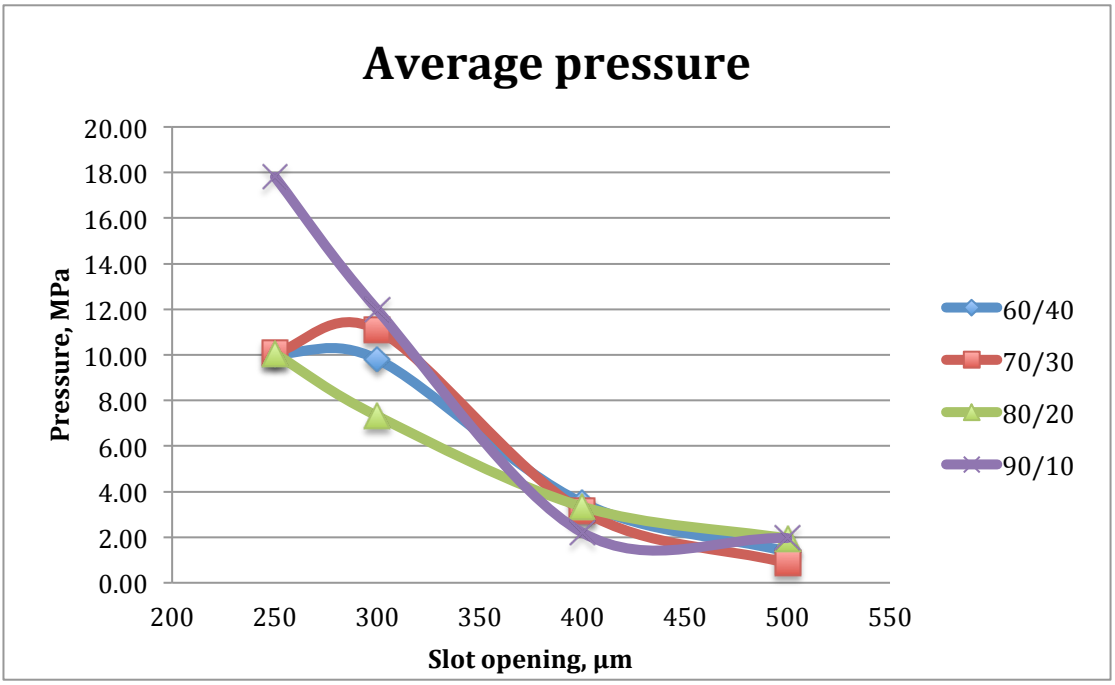

Figure 39: Data obtained for average pressure during lost circulation experiments.

4.6.3. Average peak pressure for the mud systems

Similar trends are shown for these data, when compared to the average pressure. It can be seen that while the 90/10 mud is able to resist the highest pressure out of the OBMs at 250 microns, the 70/30 OBM has a slightly higher resistance to pressure than the 90/10 OBM at 300 microns.

The resistance of the bridges for all mud systems are significantly reduced as the slot opening increases above the D50.

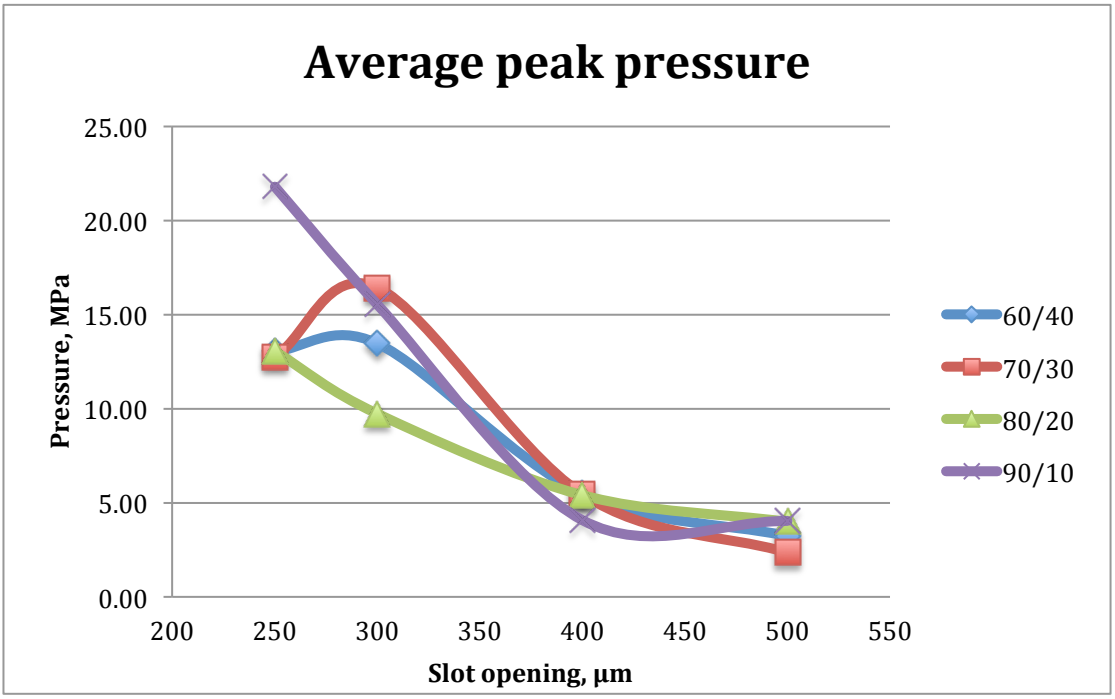

Figure 40: Data obtained for average peak pressure during lost circulation experiments.

4.6.4. Number of peaks for the mud systems

The ability of the fluid to create bridges is shown in Figure 41, although this parameter alone does not provide any information about the strength of the bridge. An observation done here is that the number of peaks declines for the 60/40 and 70/30 OBMs, while it slightly increases for the 80/20 and 90/10 OBMs during the transition from 250 micron to 300 micron. When looking at the transition from 400 micron to 500 micron, the number of peaks is reduced for all OBMs.

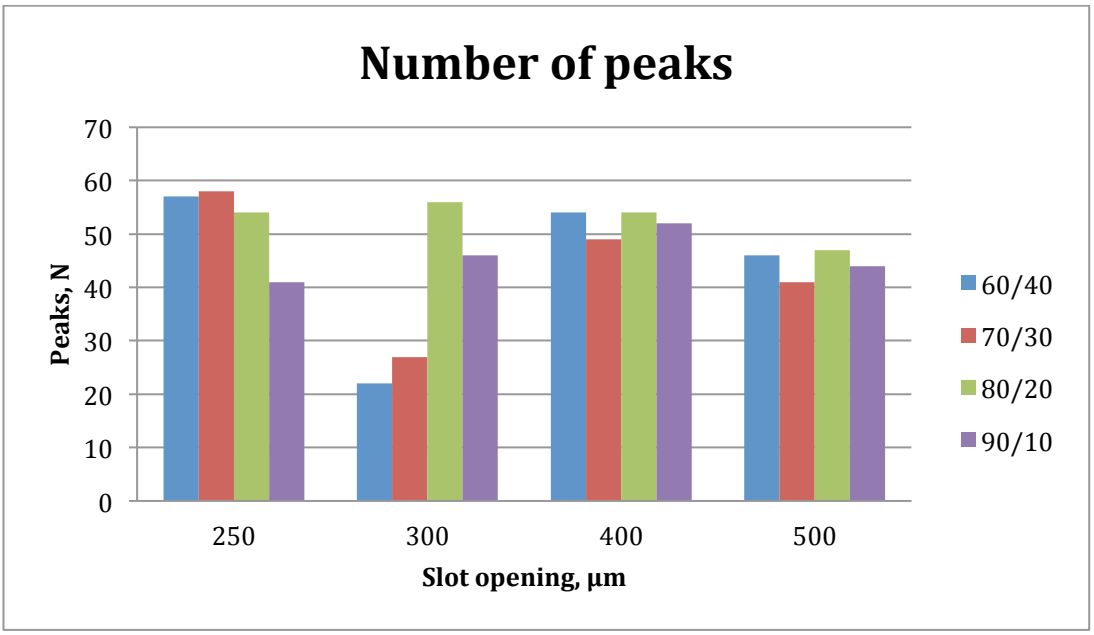

Figure 41: Data obtained for number of peaks during lost circulation experiments.

4.7. Effect of fluid rheology on fracture pressure

One of the goals of the thesis is to figure out if there is a possible correlation between the rheological properties of a drilling fluid and the sealing capacity during lost circulation. The pressure data used are presented in Table 9, and the rheological parameters used for the correlation study are provided in Table 10.

Since the tests for each mud system at a set slot opening was only performed once, a trendline will be added in order to analyse the data gathered.

Table 9: Average pressure form lost circulation experiments.

Drilling fluid	Pa 250 (MPa)	Pa 300 (MPa)	Pa 400 (MPa)	Pa 500 (Mpa)
60/40	10.063	9.808	3.512	1.368
70/30	10.097	11.102	3.157	0.858
80/20	10.058	7.318	3.339	1.942
90/10	17.797	11.982	2.201	1.961

Table 10: Rheological parameters used for analysis.

Drilling fluid	AV (cP)	PV (cP)	YS (lbs/100 ft^2)	YS/PV	n	k ($Pa*s^n$)	n/k
60/40	135	117	36	0.31	0.819	0.926	0.884
70/30	50.5	43	15	0.35	0.800	0.396	2.021
80/20	45.5	40	11	0.28	0.835	0.279	2.987
90/10	30.5	29	3	0.10	0.930	0.097	9.611

4.7.1. Average pressure versus n/k

The data obtained through lost circulation and rheology tests have been analysed in order to look into the correlation between the average pressure of the OBMs and the ratio of n and k. As seen in Figure 42, the linear trendline was the best fit in this case.

When looking at the equations generated for the trendline, it is observed that the slope between the muds differentiates as the slot opening is increased. For a slot opening of D50 (310 micron) or lower, the slope is positive, while for a slot opening that is higher than the D50 the slope is negative.

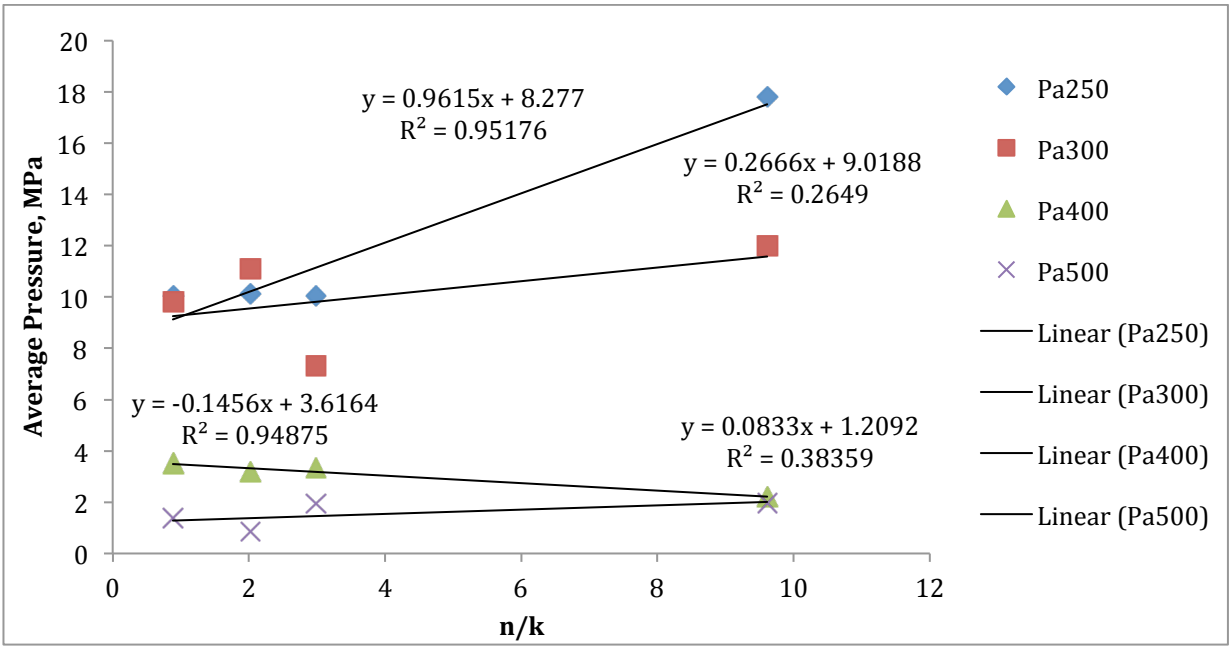

Figure 42: Comparison of the effect of n/k values on average pressure of the OBMs at different slot openings.

4.7.2. Average pressure versus plastic viscosity

During the analysis, it was observed that the correlation was less in most cases when plotting average pressure versus single rheology parameters, compared to a ratio of two parameters. An example is given in Figure 43, for the plastic viscosity.

It is observed that the R^2 value is significantly less for all slot openings, when compared to the values generated for the n/k ratio. The linear trendline was the best fit, but it does not generate reliable equations in this case.

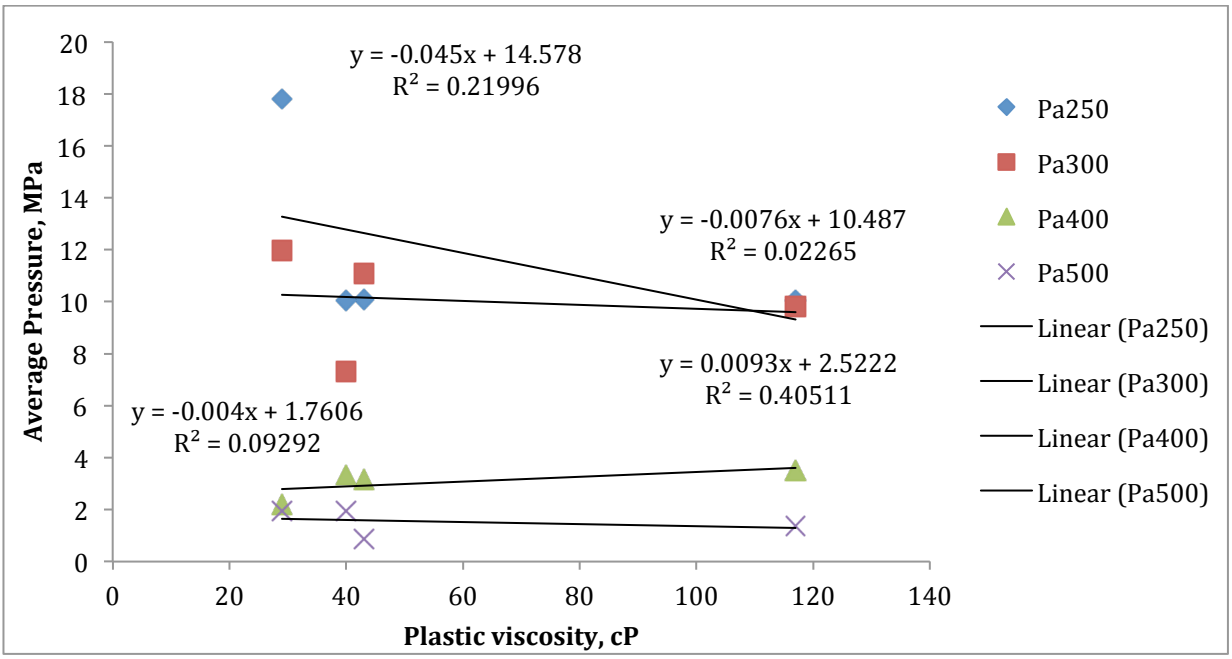

Figure 43: Comparison of the effect of PV on average pressure of the OBMs at different slot openings.

4.7.3. Correlation constant for parameters

The R^2 value has been calculated for all of the mentioned parameters, which will be used to look for correlation in the data. This value is calculated from the correlation coefficient, R, when squared. The results are presented for each of the four slot openings separately below.

From Figure 44, it is observed that the correlation is higher for the 250- and 400 slot openings. The 500 slot opening shows a decrease in correlation, while the 300 slot opening has significantly less correlation.

An interesting observation is that the parameters that show the highest R^2 value for all of the slot openings are the YS/PV, the flow behaviour index (n) and the n/k ratio.

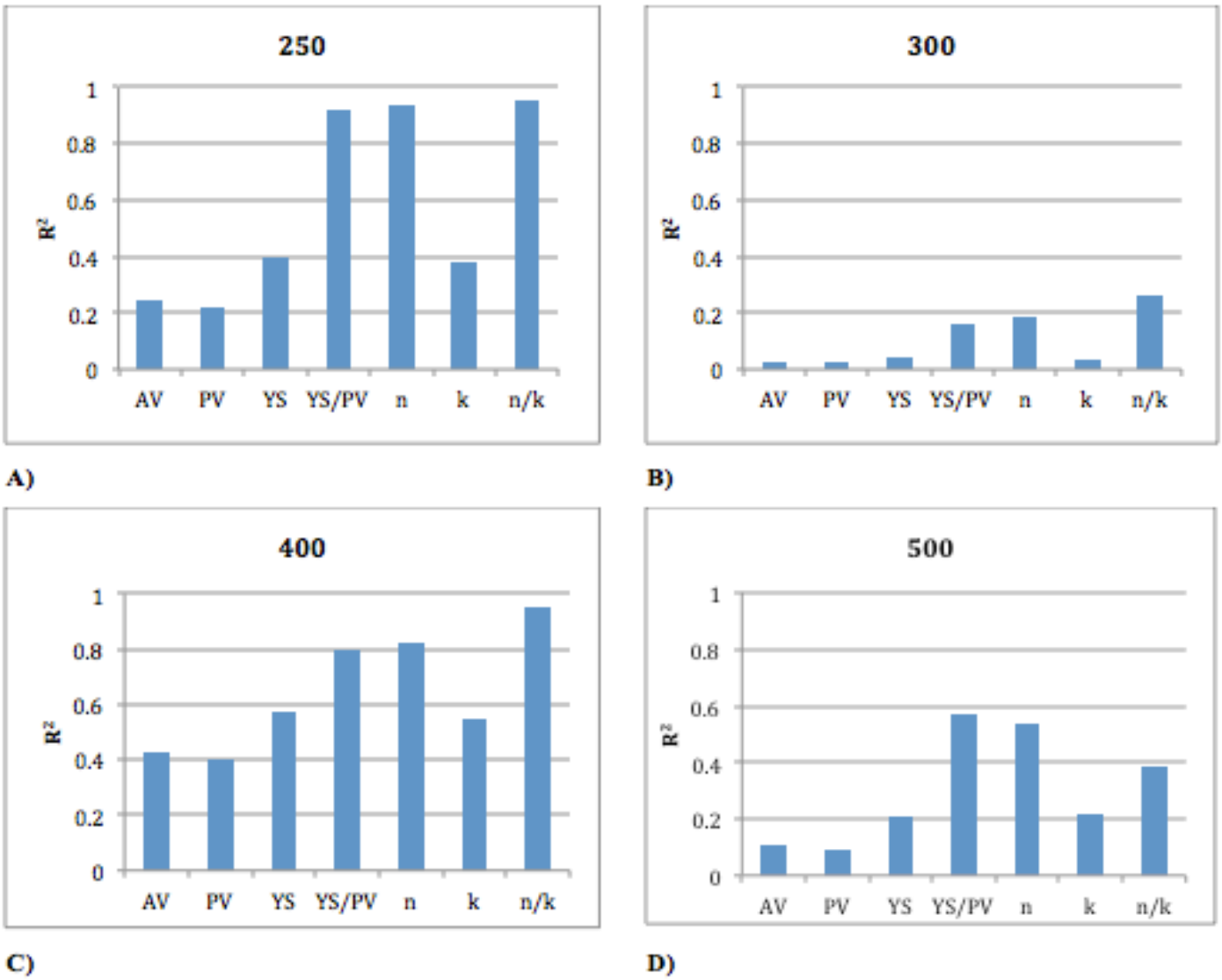

Figure 44: The R^2 value for the rheological parameters when correlated with average pressure at A) 250 micron slot opening, B) 300 micron slot opening, C) 400 micron slot opening, D) 500 micron slot opening.

5. Discussion

In this sections the overall investigations will be discussed. The majority of the experiments and simulations have been performed at room temperature (72°F) where all parameters for the fluids are known.

Effect of temperature on plastic viscosity and yield stress

During a drilling operation for a shallow well, the temperature changes will not be that large, and hence rheological variations will not be as significant. However, a deep well with a small margin between the pore and fracture pressure may need careful evaluation of the temperature effect on wellbore hydraulics. The effect of temperature was analysed and compared for four mud systems in this thesis. In the thesis it was concluded that all four mud systems were sensitive to temperature changes. A decrease was observed for most mud systems when the temperature was increased from 72°F to 180°F. The results were:

- For the PV, an increase in temperature from 72°F to 180°F led to a % decrease of 63%, 46%, 60% and 61% for the 60/40, 70/30, 80/20 and 90/10 OBM respectively.
- For the YS, the decrease is also most prominent for the 60/40 OBM. The YS from the two temperature ranges (72°F to 180°F) is close to equal for the 70/30 and 80/20 OBMs, and an increase of 3 lbs/100ft^2 is seen for the 90/10 OBM.

The equations generated for PV and YS as a function of temperature are in this thesis only valid for the given temperature ranges at atmospheric pressure. In a real well scenario, it would be preferable to study the variations of the two parameters when exposed to a variety of temperature and pressure. This would give a better presentation of how the mud systems would act in an actual well operation.

Cuttings transport performance of the mud systems

A good hole cleaning is critical in order to ensure a successful drilling operation. By removing the accumulations of cuttings in the well, and transporting them to the surface, a good hole cleaning can be accomplished. Parameters that affect the performance are mud density and rheology, cuttings parameters, and operational parameters such as angle of inclination, ROP, RPM and flow rate. The minimum (critical) flow rate as a function of inclination, and bed height at a certain flow rate were simulated in the thesis. Density, cuttings parameters and operational parameters were constant during the simulations, which allowed for an analysis of the rheological properties of the fluids.

The results from the minimum flow rate simulations were divided into two regions; region 1 (0-45°) and region 2 (45-90°). The performance of the OBMs shifted during the transition of regions, and can be summarized as:

- Region 1: 60/40 > 70/30 > 80/20 > 90/10
- Region 2: 60/40 > 70/30 > 90/10 > 80/20

The simulations of performance in terms of bed height were simulated with an experimental well with a maximum inclination of 35°. Additional well parameters were added here, and a new minimum flow rate was calculated from the results. The new minimum flow rate for the OBMs were in line with the results summarized above for region 1, considering the well inclination of this well. The performance of the OBMs in terms of bed height are summarized below:

- 60/40 > 70/30 > 80/20 > 90/10

A higher YS value and viscosity appeared to be favourable in terms of cuttings transport efficiency when looking at the rheological parameters.

Bridging performance

Lost circulation is a major problem in the industry, as it can lead to high costs for a drilling operation. The four scenarios that can cause lost circulation to occur are permeable zones, natural fractures, induced fractures and caverns. In order to combat the lost circulation problems, two separate measures exist, which are preventative and remedial measures. The experiments performed in the thesis has a focus on the remedial measure that uses lost circulation material in order to bridge the lost circulation interval.

Different particle size distributions were discussed in the theory section, and for the experiments a PSD with a D50 at 310 microns were used. The bridging performance could then be evaluated for the four mud systems when 13.82 ppb LC-lube was added. The tests were performed with various slot widths of 250, 300, 400 and 500 microns, which also allowed for an evaluation of the Halliburton Method. The pressure parameters for maximum pressure, average pressure and average peak pressure were determined in order to analyse the pressure profile for the mud systems.

The results showed that a better bridging performance was obtained when the slot size (fracture width) were 300 and 250 microns, which were close to or less than the D50 of the PSD. The strength of the bridges decreased as the slot size was increased above the D50. The average strength of the bridges in the different mud systems can be summarized as following for the performed tests at 250 and 300 micron slot openings:

- 90/10 > 70/30 > 60/40 > 80/20

Correlation between bridging pressure and rheological parameters

The average pressure data determined from the experimental tests were compared with the rheological properties of the mud systems in order to see if there were any correlations. Previous studies found on the topic have shown that there are no indications of a correlation.

From the investigation performed in this thesis, it was observed that three parameters could indicate correlations, which were the flow behaviour index, n, YS/PV ratio and the n/k ratio.

6. Conclusions

In this thesis, four different oil-based mud systems have been tested. The work performed were the following:

- Rheological measurement and characterization of the mud systems at various temperatures.
- Simulation of the hole cleaning efficiency for the mud systems.
- A static bridge apparatus was used in order to perform lost circulation experiments.

Based on the characterization and performance, the following conclusions can be drawn:

- From the rheology measurements, the results showed that the Hershel Bulkley-, Unified- and Robertson-Stiff- model had the lowest error rates, and therefore gave the best description of the 60/40, 70/30, 80/20 and 90/10 oil-based muds.
- When looking at the temperature effect on the rheological properties, it is observed that plastic viscosity has a greater variation with temperature than yield stress.
- From the simulations performed for cuttings transport on the four mud systems, the 60/40 OBM has the lowest minimum flow rate required to remove cuttings to surface.
- Furthermore, the bed height is lower for the 60/40 OBM when simulations were performed with a flow rate of 400 gpm. The bed height simulations concluded with a performance of the OBMs in the following order:

  60/40 > 70/30 > 80/20 > 90/10

From the lost circulation experiments with a fluid additive of 13.82 ppb LC-lube, it was concluded that:

- Better performance when the D50 of the particle distribution is closer to, or higher than the slot opening used, for all mud systems, as proposed by the Halliburton Method (Whitfill, 2008).
- Less stable bridges for the 400- and 500-micron slot openings, since the slot sizes are higher than the D50 of the PSD.
- Three rheological parameters were found to indicate correlation to with average pressure for the given mud systems. The parameters were the n, YS/PV and n/k ratio.

7. Future work

In order to verify that there is a possible correlation between the mentioned rheological parameters with fracture pressure, several tests should be performed with a fluid in order to normalize the pressure readings.

References

1. Aadnøy, B. S., 1998. *Geomechanical Analysis for Deep-Water Drilling.* IADC/SPE Drilling Conference, Dallas, Texas.
2. Aadnøy, B. S., 2010. *Modern well design*. 2nd ed. CRC Press/Balkema, London, UK.
3. Abimbola, M. O., Chukwu, G. A., Khan, F. I., 2014. *Cuttings Transport Evaluation in Deviated Wells.* International Conference on Marine and Freshwater Environments, St. John's, Canada.
4. Abrams, A., 1977. *Mud Design to Minimize Rock Impairment Due To Particle Invasion*. Journal of Petroleum Technology, 29:5, p. 586-592.
5. Alberty, M. W. and McLean, M. R., 2004. *A Physical Model for Stress Cages*. SPE Annual Technical Conference and Exhibition, Houston, Texas.
6. Aston, M. S., Alberty, M. W., McLean, M. R., de Jong, H. J. and Armagost, K., 2004. *Drilling Fluids for Wellbore Strengthening*. IADC/SPE Drilling Conference, Dallas, Texas.
7. Avasthi, J. M., Goodman, H. E. and Jansson R. P., 2000. *Acquisition, Calibration, and Use of the In Situ Stress Data for Oil and Gas Well Construction and Production*. SPE Rocky Mountain Regional/Low-Permeability Reservoirs Symposium and Exhibition, Denver, Colorado.
8. Azar, J. J. and Robello Samuel, G., 2007. *Drilling Engineering*. PennWell Corporation, Tulsa, Oklahoma.
9. Baker Hughes, 2007. *LC-LUBE™ FINE.* Available at: http://www.shopbakerhughes.com/media/pdf/LC-LUBE_FINE_ProductBulletin.pdf (Last accessed 09 June 2015).
10. Belayneh, M., 2004. *Experimental and Analytical Borehole Stability Study*. Ph.D. Thesis, Høgskolen i Stavanger.
11. Bourgoyne Jr., A. T., Millheim, K. K., Chenevert, M. E. and Young Jr., F. S., 1986. Applied Drilling Engineering. SPE Textbook Series, Vol. 2. Society of Petroleum Engineers, Richardson, Texas.
12. Caenn, R., Darley, H. C. H. and Gray, G. R, 2011. *Composition and Properties of Drilling and Completion Fluids*. 6th ed. Elsevier, Waltham, USA.

13. Darley, H. C. H. and Gray, G. R., 1988. *Composition and Properties of Drilling and Completion Fluids.* 5th ed. Gulf Publishing Company, Houston, Texas.
14. Dick, M. A., Heinz, T. J. and Svoboda, C. F. and Aston, M., 2000. *Optimizing the Selection of Bridging Particles for Reservoir Drilling Fluids*. SPE International Symosium on Formation Damage Control, Lafayette, Louisiana.
15. Dupriest, F. E., 2005. *Fracture Closure Stress (FCS) and Lost Returns Practices*. SPE/IADC Drilling Conference, Amsterdam, Netherlands.
16. Economides, M. J., Watters, L. T. and Dunn-Norman, S., 1998. *Petroleum Well Construction*. John Wiley & Sons, Ltd, Chichester, England.
17. Gerner, A., 2012. *Lost circulation experimental study in Oil Based mud and analyzing experimental data.* MSc Thesis, University of Stavanger.
18. Gulsrud, T. O., Nybø, R., Bjørkevoll, K. S., 2009. *Statistical Method for Detection of Poor Hole Cleaning and Stuck Pipe.* SPE Offshore Europe Oil & Gas Conference & Exhibition, Aberdeen, UK.
19. Khaing, S. W. A., 2014. Characterization and Performance of 70/30 and 90/10 OBM mud systems. MSc Thesis, University of Stavanger.
20. Looyeh, R. and Aadnøy, B. S., 2011. *Petroleum Rock Mechanics: Drilling Operations and Well Design*. 1st ed. Gulf Professional Publishing, Oxford, United Kingdom.
21. Mitchell, R. F. and Miska, S. Z., 2011. *Fundamentals of drilling engineering*. SPE Textbook Series, Vol. 12. Society of Petroleum Engineers, Richardson, Texas.
22. Ochoa, M. V., 2006. *Analysis of drilling fluid rheology and tool joint effect to reduce errors in hydraulics calculations*. Ph.D. Thesis, Texas A&M University.
23. Okrajni, S. S. and Azar, J. J. 1986. *The Effects of Mud Rheology on Annular Hole Cleaning in Directional Wells*. SPE Drilling Engineering, 01:04, p. 297-308.
24. Robertson, R. E. and Stiff, H. A., 1976. *An Improved Mathematical Model for Relating Shear Stress to Shear Rate in Drilling Fluid and Cement Slurries*. Society of Petroleum Engineers Journal, 16:1, p. 31-36.

25. Savari, S., Whitfill, D. L. and Kumar, A., 2012. *Resilient Lost Circulation Material (LCM): A Significant Factor in Effective Wellbore Strengthening*. SPE Deepwater Drilling and Completions Conference, Galveston, Texas.
26. Sifferman, T. R., Myers, G. M., Haden, E. L. and Wahl, H. A., 1974. *Drill Cutting Transport in Full Scale Vertical Annuli.* Journal of Petroleum Technology, 26:11.
27. Skjeggestad, O., 1989. *Boreslam teknologi*. Alma Mater Forlag AS, Bergen.
28. Statoil ASA, 2010. *Activity Program Drilling Well NO 6608/10-K-2 H & AH NORNE*.
29. Thorbjornsen, K., 2009. *Brønnvæsketeknologi*. Vett & Viten ELS, Høvik.
30. Toroqi, S. V. M., 2012. *Experimental Analysis and Mechanistic Modeling of Wellbore Strengthening*. Ph.D. Thesis, University of Calgary.
31. Versan, M. and Tolga, A, 2005. *Effect of Polymers on the Rheological properties of KCl/Polymer Type Drilling Fluids*. Energy Sources, 27:5, p. 405-415.
32. Vickers, S., Cowie, M., Jones, T. and Twynam, A. J., 2006. *A new methodology that surpasses current bridging theories to efficiently seal a varied pore throat distribution as found in natural reservoir formations*. AADE-06-DF-HO-16. American Association of Drilling Engineers, 23:1, p. 501-515.
33. Vieira, M. G. and Peres, A. E. C., 2012. *Effect of Reagents on the Rheological Behavior of an Iron Ore Concentrate Slurry*. International Journal of Mining Engineering and Mineral Processing, 1(2): p. 38-42.
34. Whitfill, D., 2008. *Lost Circulation Material Selection, Particle Size Distribution and Fracture Modeling with Fracture Simulation Software*. IADC/SPE Asia Pacific Drilling Technology Conference and Exhibition, Jakarta, Indonesia.
35. Zamora, M. and Power, D., 2002. *Making a Case for AADE Hydraulics and the Unified Rheological Model*. AADE 2002 Technology Conference "Drilling & Completion Fluids and Waste Management", Houston, Texas.
36. Zamora. M., Roy, S. and Slater, K., 2005. *Comparing a Basic Set of Drilling Fluid Pressure-Loss Relationships to Flow-Loop and Field Data.* AADE 2005 National Technical Conference and Exhibition, Houston, Texas.

Appendix

Appendix A: Rheology models and parameters

In order to determine the rheology model that is the best match, the shear stress is calculated for each model, and then compared with the data obtained from laboratory experiments. The % error between the different rheology models and the original data denotes which model is the best match for the mud systems. The data obtained and calculated are shown in the tables below.

Rheology data and calculations of 60/40 OBM at room temperature (72°F)

		Parameters				
Model	Equation	τo,τy, A	k, C	n, B	μp, μ	Error
Herschel Bulkley	0.6389*γ^0.8763+14.02	14.020	0.6389	0.8763		1.38
Unified	13.871+0.6794*γ^0.8665	13.871	0.6794	0.8665		1.13
Power Law	6.0404*γ^0.527		6.0404	0.527		12.36
Bingham	0.266*γ+21.886	21.886			0.266	14.62
Newtonian	0.297*γ				0.297	38.88
Robertson-Stiff	0.9974*(27.1372+γ)^0.8122	0.9974	27.1372	0.8122		1.43

The viscosity determined from the rheology models are in the unit lbf s/ft^2, but converted into cP by multiplying with 478.80:

Plastic viscosity (Bingham): $\mu_p = 0.266*478.80 = 127.361$ cP

Newtonian viscosity: $\mu = 0.297*478.80 = 142.204$ cP

Rheology data and calculations of 60/40 OBM at room temperature (120°F)

		Parameters				
Model	Equation	τo,τy, A	k, C	n, B	μp, μ	Error
Herschel Bulkley	0.5918*γ^0.82+10.827	10.827	0.5918	0.8200		2.64
Unified	10.137+0.8112*γ^0.7696	10.137	0.8112	0.7696		2.89
Power Law	5.1576*γ^0.4864		5.1576	0.4864		11.26
Bingham	0.1701*γ+17.105	17.105			0.1701	13.66
Newtonian	0.1944*γ				0.1944	40.65
Robertson- Stiff	0.9436*(27.9422+γ)^0.7553	0.9436	27.9422	0.7553		3.19

Plastic viscosity (Bingham): $\mu_p = 0.1701*478.80 = 81.444$ cP

Newtonian viscosity: $\mu = 0.1944*478.80 = 93.079$ cP

Rheology data and calculations of 60/40 OBM at room temperature (180°F)

		Parameters				
Model	Equation	τo,τy, A	k, C	n, B	μp, μ	Error
Herschel Bulkley	0.4691*γ^0.7858+10.717	10.717	0.4691	0.7858		1.99
Unified	10.670+0.4844*γ^0.7807	10.670	0.4844	0.7807		1.87
Power Law	5.586*γ^0.4111		5.586	0.4111		10.35
Bingham	0.1022*γ+16.681	16.681			0.1022	16.04
Newtonian	0.1259*γ				0.1259	45.71
Robertson-Stiff	1.1832*(30.9819+γ)^0.6564	1.1832	30.9819	0.6564		2.08

Plastic viscosity (Bingham): $\mu_p = 0.1022*478.80 = 48.933$ cP

Newtonian viscosity: $\mu = 0.1259*478.80 = 60.281$ cP

Rheology data and calculations of 70/30 OBM at room temperature (72°F)

		Parameters				
Model	Equation	τo,τy, A	k, C	n, B	μp, μ	Error
Herschel Bulkley	0.2516*γ^0.8679+6.5033	6.50333	0.2516	0.8679		1.38
Unified	6.402+0.2799*γ^0.8507	6.402	0.2799	0.8507		0.81
Power Law	2.9057*γ^0.4898		2.9057	0.4898		12.28
Bingham	0.0982*γ+9.7734	9.7734			0.0982	14.01
Newtonian	0.1121*γ				0.1121	40.69
Robertson-Stiff	0.4256*(32.6237+γ)^0.7931	0.4256	32.6237	0.7931		1.14

Plastic viscosity (Bingham): $\mu_p = 0.0982*478.80 = 47.018$ cP

Newtonian viscosity: $\mu = 0.1121*478.80 = 53.673$ cP

Rheology data and calculations of 70/30 OBM at room temperature (120°F)

		Parameters				
Model	Equation	τo,τy, A	k, C	n, B	μp, μ	Error
Herschel Bulkley	0.2845*γ^0.8104+6.492	6.492	0.2845	0.8104		1.72
Unified	6.402+0.3125*γ^0.7954	6.402	0.3125	0.7954		1.36
Power Law	3.2178*γ^0.4404		3.2178	0.4404		10.79
Bingham	0.074*γ+10.188	10.188			0.074	15.99
Newtonian	0.0884*γ				0.0884	44.11
Robertson-Stiff	0.6101*(30.993+γ)^0.7031	0.6101	30.9930	0.7031		1.76

Plastic viscosity (Bingham): μ_p = 0.074*478.80 = 35.43 cP

Newtonian viscosity: μ = 0.0884*478.80 = 42.326 cP

Rheology data and calculations of 70/30 OBM at room temperature (180°F)

		Parameters				
Model	Equation	τo,τy, A	k, C	n, B	μp, μ	Error
Herschel Bulkley	0.2151*γ^0.8233+6.630	6.630	0.2151	0.8233		2.51
Unified	6.936+0.1301*γ^0.9041	6.936	0.1301	0.9041		4.46
Power Law	3.3439*γ^0.4076		3.3439	0.4076		10.87
Bingham	0.059*γ+10.064	10.064			0.059	17.14
Newtonian	0.0733*γ				0.0733	46.42
Robertson-Stiff	0.693*(31.8766+γ)^0.6562	0.693	31.8766	0.6562		1.30

Plastic viscosity (Bingham): μ_p = 0.059*478.80 = 28.249 cP

Newtonian viscosity: μ = 0.0733*478.80 = 35.096 cP

Rheology data and calculations of 80/20 OBM at room temperature (72°F)

		Parameters				
Model	Equation	τo,τy, A	k, C	n, B	μp, μ	Error
Herschel Bulkley	0.1571*γ^0.923+4.848	4.848	0.1571	0.9230		0.84
Unified	4.908+0.1425*γ^0.9387	4.908	0.1425	0.9387		1.32
Power Law	1.9695*γ^0.529		1.9695	0.529		14.17
Bingham	0.09*γ+6.730	6.730			0.09	11.33
Newtonian	0.0995*γ				0.0995	37.75
Robertson-Stiff	0.2401*(33.2137+γ)^0.8612	0.2401	33.2137	0.8612		0.47

Plastic viscosity (Bingham): μ_p = 0.09*478.80 = 43.092 cP

Newtonian viscosity: μ = 0.0995*478.80 = 47.641 cP

Rheology data and calculations of 80/20 OBM at room temperature (120°F)

		Parameters				
Model	Equation	τo,τy, A	k, C	n, B	μp, μ	Error
Herschel Bulkley	0.1491*γ^0.8675+3.669	3.669	0.1491	0.8675		1.74
Unified	3.735+0.1315*γ^0.8876	3.735	0.1315	0.8876		2.24
Power Law	1.6276*γ^0.4978		1.6276	0.4978		12.38
Bingham	0.0584*γ+5.522	5.522			0.0584	13.93
Newtonian	0.0662*γ				0.0662	40.12
Robertson-Stiff	0.2782*(28.4766+γ)^0.7775	0.2782	28.4766	0.7775		1.92

Plastic viscosity (Bingham): μ_p = 0.0584*478.80 = 27.962 cP

Newtonian viscosity: μ = 0.0662*478.80 = 31.697 cP

Rheology data and calculations of 80/20 OBM at room temperature (180°F)

		Parameters				
Model	Equation	τo,τy, A	k, C	n, B	μp, μ	Error
Herschel Bulkley	0.1221*γ^0.84810+4.73	4.730	0.1221	0.8481		3.31
Unified	4.908+0.0747*γ^0.9271	4.908	0.0747	0.9271		5.20
Power Law	2.3628*γ^0.399		2.3628	0.399		11.06
Bingham	0.0393*γ+6.904	6.904			0.0393	16.18
Newtonian	0.0491*γ				0.0491	46.60
Robertson-Stiff	0.4046*(38.3213+γ)^0.6768	0.4046	38.3213	0.6768		1.07

Plastic viscosity (Bingham): μ_p = 0.0393*478.80 = 18.817 cP

Newtonian viscosity: μ = 0.0491*478.80 = 23.509 cP

Rheology data and calculations of 90/10 OBM at room temperature (72°F)

		Parameters				
Model	Equation	τo,τy, A	k, C	n, B	μp, μ	Error
Herschel Bulkley	0.0954*γ^0.9364+2.421	2.421	0.0954	0.9364		2.18
Unified	2.561+0.0638*γ^1.0013	2.561	0.0638	1.0013		3.34
Power Law	0.9311*γ^0.5792		0.9311	0.5792		13.82
Bingham	0.0608*γ+3.296	3.296			0.0608	10.03
Newtonian	0.0655*γ				0.0655	34.54
Robertson-Stiff	0.1463*(24.7558+γ)^0.8727	0.1463	24.7558	0.8727		2.52

Plastic viscosity (Bingham): μ_p = 0.0608*478.80 = 29.111 cP

Newtonian viscosity: μ = 0.0655*478.80 = 31.361 cP

Rheology data and calculations of 90/10 OBM at room temperature (120°F)

		Parameters				
Model	Equation	τo,τy, A	k, C	n, B	μp, μ	Error
Herschel Bulkley	0.0733*γ^0.92310+2.347	2.347	0.0733	0.9231		1.11
Unified	2.347+0.0731*γ^0.9235	2.347	0.0731	0.9235		1.13
Power Law	0.9594*γ^0.5227		0.9594	0.5227		14.12
Bingham	0.0417*γ+3.307	3.307			0.0417	12.13
Newtonian	0.0464*γ				0.0464	38.37
Robertson-Stiff	0.1078*(35.5807+γ)^0.8673	0.1078	35.5807	0.8673		0.50

Plastic viscosity (Bingham): μ_p = 0.0417*478.80 = 19.966 cP

Newtonian viscosity: μ = 0.0464*478.80 = 22.216 cP

Rheology data and calculations of 90/10 OBM at room temperature (180°F)

		Parameters				
Model	Equation	τo,τy, A	k, C	n, B	μp, μ	Error
Herschel Bulkley	0.0805*γ^0.8473+2.394	2.394	0.0805	0.8473		2.01
Unified	2.241+0.128*γ^0.7731	2.241	0.128	0.7731		2.76
Power Law	1.1406*γ^0.4417		1.1406	0.4417		12.94
Bingham	0.0273*γ+3.433	3.433			0.0273	12.39
Newtonian	0.0322*γ				0.0322	42.92
Robertson-Stiff	0.1224*(46.0063+γ)^0.7915	0.1224	46.0063	0.7915		1.99

Plastic viscosity (Bingham): μ_p = 0.0273*478.80 = 13.071 cP

Newtonian viscosity: μ = 0.0322*478.80 = 15.417 cP

Appendix B: Hole data and drill string data for simulation of cuttings transport

The hole and drill string data used for simulation of cuttings transport is provided below.

Hole data (casing and open hole)

Table B.1: Hole data for simulation.

Section type	Measured depth (ft)	Length (ft)	Shoe measured depth (ft)	ID (in)	Drift (in)	Effective hole diameter (in)	Friction factor	Linear capacity (bbl/ft)	Item description
Casing	4012.5	4012.5	4012.5	12.250	12.459	12.615	0.25	0.1547	13 3/8 in, 54.5 ppf, J-55
Open hole	11003.3	6990.8		12.250		12.250	0.3	0.1546	

Drill string data (Drill pipe and BHA)

Table B.2: Drill string data for simulation.

Section type	Lenth (ft)	Measured depth (ft)	OD (in)	ID (in)	Weight (ppf)	Item description
Drill pipe	10445.3	10445.3	5	4.276	22.26	Drill pipe 5 in, 19.50 ppf, E, 5 ½ FH, P
Heavy Weight	120.0	10565.3	6.625	4.5	70.5	Heavy weight drill pipe Grant Prideco, 6 5/8 in, 70.50 ppf
Jar	32.0	10597.3	6.5	2.75	91.79	Hydraulic jar Dailey Hyd., 6 ½ in
Heavy Weight	305.0	10902.3	5.0	3.0	49.7	Heavy weight drill pipe Grant Prideco, 5 in, 49.70 ppf
Sub	5.0	10907.3	6.0	2.4	79.51	Bit sub 6, 6 x2 ½ in
MWD	85.0	10992.3	8.0	2.5	154.36	MWD tool 8, 8 x2 ½ in
Stabilizer	5.0	10997.3	6.25	2.0	93.72	Integral blade stabilizer 8 ½ in FG, 6 ¼ x2 in
Sub	5.0	11002.3	6.0	2.4	79.51	Bit sub 6, 6 x2 ½ in
Bit	1.0	11003.3	10.625		166	Tri-Cone bit, 0.589 in^2

Appendix C: Determination of flow regime for cuttings transport simulations

In order to determine the flow regime in the annulus during the cuttings transport, the Unified rheology model for hydraulics calculations was used. A generalized Reynolds number can be found by using the equations defined by Zamora et al. (2005). The equations and the calculated results for annular flow regime are presented below.

Reynolds number:

$$N_{Re} = \frac{\rho {v_a}^2}{19.36 * \tau_W} \quad \text{(C.1)}$$

Where

$N_{Re} < 2100$ indicates laminar flow, and $N_{Re} > 4000$ indicates turbulent flow.

Velocity:

$$v_a = \frac{24.5q}{{D_2}^2 - {D_1}^2} \quad \text{(C.2)}$$

Correction factor:

$$G = \left(\frac{2n+1}{3n}\right) \times 1.5 \quad \text{(C.3)}$$

Shear rate at the wall:

$$\gamma_W = \frac{1.6 G v_a}{D_2 - D_1} \quad \text{(C.4)}$$

Shear stress at the wall:

$$\tau_W = \left(\frac{3}{2}\right)^n \tau_{yL} + k {\gamma_W}^n \quad \text{(C.5)}$$

By using the well parameters given in Appendix B, the flow regime was calculated for the different sections of the well, presented in Table. The values show that the flow regime is laminar for all four mud systems in the annulus.

Table C.1: Reynolds number for the four mud systems in annulus.

Reynolds number				
Section type	**60/40 OBM**	**70/30 OBM**	**80/20 OBM**	**90/10 OBM**
Drill pipe (casing)	149.15	346.27	439.13	844.55
Drill pipe	134.48	310.75	394.94	759.65
Heavy Weight	152.83	375.68	473.73	909.49
Jar	157.49	369.31	466.06	895.09
Heavy Weight	134.48	310.75	394.94	759.65
Sub	148.54	346.38	438.35	842.69
MWD	194.86	467.21	582.27	1108.30
Stabilizer	152.83	357.36	451.64	867.88
Sub	148.54	346.38	438.35	842.69
Bit	326.24	836.95	986.91	1716.17